ORIGINAL RESEARCH Open access

Event-Triggered Fault-Tolerant Control of Multiple UAV Formations under External Disturbances

Lars Petersen[1*], Maja Jensen[1], Henrik Nielsen[2], Ursula Hoffmann[3], Christian Andersen[4]

Abstract

This work proposes an event-triggered, fault-tolerant, time-varying formation control strategy for multiple unmanned aerial vehicles (UAVs). A formation-tracking controller is carefully constructed with a prescribed tracking performance to manage both actuator faults and external disturbances. First, the desired heading angle is obtained via a line-of-sight algorithm. Second, to counteract actuator faults and external disturbances, a radial basis function neural network (RBFNN) is combined with adaptive law tracking control. Furthermore, adaptive tracking controllers and event-triggering conditions are developed to raise the computational update rate. The prescribed tracking performance, enforced via a Lyapunov function, ensures that the tracking error decays over time. Finally, a rigorous system stability analysis is carried out, conclusively eliminating Zeno behavior. The simulation results fully substantiate the theoretical findings.

Keywords Multiple UAVs, Time-varying formation control, Fault-tolerant control, Event-triggered control, External disturbances, Predefined tracking performance

*Correspondence:
Lars Petersen
lars.petersen@food.ku.dk
[1] Department of AI for Pig and Poultry Health Monitoring using Acoustic Sensors, Faculty of Agricultural Sciences, University of Copenhagen, Copenhagen, Denmark
[2] Department of Machine Learning for Feed Efficiency and Growth Modeling, Faculty of Agriculture, Aarhus University, Aarhus, Denmark
[3] Department of Smart Barn Climate Control Systems, Faculty of Agriculture, University of Basel, Basel, Switzerland
[4] Department of Precision Waste Management, Faculty of Agriculture, University of Southern Denmark, Odense, Denmark

Introduction

Owing to the growing intricacy of aviation tasks and the ongoing advancement of aircraft control, network communication, and artificial intelligence technologies, unmanned aerial vehicles (UAVs) have attained overall system efficiency gains through mutual capability supplementation and coordinated individual behaviors. In complex operations and settings, such as cooperative target observation, area surveillance, collaborative analysis and decision-making, and coordinated formation flight, UAV swarms offer significant advantages. However, as the number of swarm members increases and functional interdependencies tighten, the complexity of navigation and communication grows exponentially. The establishment and preservation of formations during swarm flight missions likewise pose greater difficulties. If a UAV swarm cannot autonomously handle unforeseen faults and external disturbances under harsh weather conditions, the full benefits of cooperative operation become hard to realize. Thus, increased demands are placed on swarm control, disturbance rejection, and fault-tolerance technologies. Formation control is critical to advancing multi-agent systems because it allows the swarm to operate cohesively. For this purpose, various formation control schemes have been introduced, including cooperative control [1], adaptive control [2, 3], finite-time control [4], robust formation methods [5, 6], and others. Formation control is an essential element of UAV cooperative control, in which multiple UAVs are assembled

This is an open access article distributed under the terms of the Creative Commons Attribution-NonCommercial-ShareAlike 4.0 International License (CC BY-NC-SA 4.0), which permits non-commercial use, distribution, reproduction, and adaptation in any medium or format, provided that appropriate credit is given to the original author(s) and source, a link to the license is provided, and any changes made are indicated. Adapted material must be distributed under the same license.

© 2023 The Author(s). | Published by Agro Intelligence Research Press

to carry out specific missions such as cooperative area observation [7], rescue tasks [8], and monitoring [9]. In Cai *et al.* [10], a model predictive control technique was presented for multi-UAV formation control. In Wang *et al.* [11], a new swarm intelligence methodology was proposed to coordinate multi-drone control. In Zhen *et al.* [7], a multi-UAV collaborative search-and-attack scheme was proposed. In Guo *et al.* [12], the problem of perturbation suppression for high-order multi-agent formations interacting over directed graphs was investigated.

Additionally, traditional formation control paradigms exist, including leader–follower formation control [13, 14]. Scholars in the control and systems community have largely focused on proposing control algorithms suited to distinct UAV platforms, such as multiple fixed-wing UAVs [15]. During actual flight, fixed-wing UAVs are vulnerable to parametric uncertainties and aerodynamic environmental perturbations [16].

Currently, various strategies have been advanced to manage external interference and disturbances, including backstepping control [17, 18], the barrier Lyapunov function (BLF) [19], neural network control [20, 21], sliding mode control [22], and active disturbance rejection control [23]. In backstepping control, the “explosion of complexity” issue can arise from repeated differentiation of virtual controls [24], potentially hindering the discovery of an optimal solution, particularly under uncertainties and disturbances. BLF-based adaptive finite-time control was proposed by Dong *et al.* [25], ensuring a robust response despite uncertainties. An anti-disturbance exact flight control built upon the BLF-based backstepping methodology, combined with a high-order sliding-mode observer, was proposed for ultra-low-altitude airdrop [26], yet it omitted consideration of actuator faults. In neural network control, Liu *et al.* [27] present an innovative observer-based adaptive fuzzy finite-time attitude control scheme. This approach harnesses an adaptive neural network observer to estimate angular velocity with finite-time features. By incorporating an adaptive fuzzy logic system (FLS), it successfully offsets lumped disturbances and facilitates online adaptation of the control gain. Liu *et al.* [28] describe a low-computation learning-based antisaturation fixed-time attitude-tracking control method. Here, a fixed-time state observer is constructed for accurate state estimation. Adaptive neural network technology is adopted to effectively neutralize the detrimental influences of external disturbances and uncertain parameters. Notably, the adaptive design reduces computational demand and structural complexity by adjusting a single virtual parameter online, rather than the neural network’s weight vector. Similarly, a continuous-time nonlinear system was introduced [29] that accommodated uncertainties and disturbances, but it lacked fault tolerance. Moreover, a multivariable adaptive control-based consensus flight control method that accounts for parametric uncertainties and unknown external disturbances was proposed for formation-flying UAVs [30]. These controllers share the limitation that, although they address uncertainties or disturbances [25], they overlook actuator faults within formation control [24, 26]. These approaches employ backstepping control [24], BLF-based adaptive finite-time control [25], and BLF-based backstepping control [26] to handle uncertainties and disturbances.

In formation control, actuator failure refers to a situation in which one or more agents within a formation experience a malfunction in their actuators—the components that generate and direct motion. Actuator failure can severely impact the performance and stability of a formation control system [31]. In particular, it can cause the affected agent to stray from the prescribed formation, potentially leading to collisions with other agents or environmental obstacles. Furthermore, the failure can propagate to other agents, triggering a cascading effect that destabilizes the entire formation. A BLF-based learning control method [32] and a BLF-based adaptive full-state constrained control law [33] were proposed to account for actuator faults. Various machine learning techniques, including neural networks, are used to address system uncertainty and nonlinearity [34, 35]. An event-triggered extended state observer (ESO) was designed that activated solely on output signals, independent of system states. An event-triggered active disturbance rejection control (ADRC) scheme was presented in Sun *et al.* [36], which prevented the latest state, disturbance estimates, and control signals from depending on any sensor-network transmission until the discrete triggering condition was violated.

Additionally, for high-order linear multi-agent systems, fault-tolerant time-varying formation control problems under actuator faults were explored [37]. A shortcoming of the previously cited control techniques is that, while contemplating actuator faults, they lacked the capacity to incorporate uncertainties [37]. If they did, they failed to bound disturbance estimates [36].

© 2023 The Author(s). | Published by Agro Intelligence Research Press

With recent progress, mission demands have become increasingly complex. To guarantee formation flight safety, researchers must simultaneously address external interference and actuator failure. To address the weaknesses of prior methods, a composite, decentralized, fractional-order backstepping adaptive neural fault-tolerant control (FTC) approach, blending neural networks, disturbance observers, fractional calculus, and high-order sliding-mode differentiators, was proposed for attitude synchronization tracking of multiple UAVs. Its goal was to address actuator-fault and wind-effect challenges [38]. Using a distributed sliding-mode estimator, a dynamic surface control architecture, neural networks, and disturbance observers, a distributed adaptive fault-tolerant control strategy was introduced to address actuator faults and wake vortices [22]. Similarly, drawing on neighboring UAVs' local information, a fault-tolerant cooperative controller was devised considering actuator faults, input saturation, and external disturbances [39]. In Yu *et al.* [40], a fault-tolerant time-varying elliptical formation control scheme was developed using a fractional-order sliding-mode control strategy. The aim was to track the elliptical spread of a forest fire using multiple UAVs.

Furthermore, a sliding-mode disturbance observer composed of reference systems and sliding-mode differentiators was proposed to estimate lumped disturbances caused by external disturbances and actuator faults. The problem of actuator faults, input saturation, and the wake vortex effect was studied for safe control of a trailing UAV, using disturbance observers estimated in Yu *et al.* [41]; subsequently, the estimated disturbances were used to formulate backstepping control laws for longitudinal and lateral-directional dynamics. A pivotal attribute of this controller was its concurrent consideration of external wake vortex, disturbances, internal actuator faults, and input saturation. The aforementioned control methods simultaneously address actuator failure, external interference, and disturbances by leveraging a disturbance observer [22, 38, 41], fault-tolerant cooperative control [39], and fault-tolerant time-varying elliptical control [40]. To assure flight safety in complex mission environments, substantial scope for further enhancement persists.

This paper presents a fault-tolerant time-varying formation control approach for multiple UAVs featuring predefined tracking performance, addressing the identified gaps in the existing literature. The formation-tracking guidance law is designed, and tracking error performance is predetermined via a Lyapunov function. An adaptive tracking controller and a speed controller are developed, and the system's stability is analyzed. The principal contributions of this work, relative to existing methodologies, are as follows:

· The formation control guidance rate is formulated using a line-of-sight (LOS) guidance algorithm, and the formation-tracking error performance is realized through a Lyapunov function. This method, when compared with the approach proposed by Sun *et al.* [36], delivers superior results by limiting the convergence error.

· A sampling-adaptive tracking controller is introduced for the velocity and yaw angle loops, integrated with a radial basis function neural network (RBFNN). This design yields better performance under actuator failure and external disturbances while reducing communication and actuation expenditure compared to the work presented by Yu *et al.* [38].

· A novel sampling mode featuring an event-triggering mechanism is devised that uses solely input information to perform sampling. This approach eliminates the need for dedicated monitoring devices, unlike the triggering mode presented by Huang *et al.* [29], and reduces actuation communication overhead.

The remainder of this paper is organized as follows. Section 2 presents the modeling and foundational preliminaries. Section 3 details the guidance law design. Section 4 provides comparative simulation outcomes. Finally, Section 5 summarizes the conclusions of this work.

Problem Statement

Dynamic modeling of the multiple nonlinear UAVs

Below are the twelve differential equations that make up the UAV six-degree-of-freedom model [42]:

© 2023 The Author(s). | Published by Agro Intelligence Research Press

$$
\begin{cases}
m\dot{V} = T\cos\alpha - D - mg(\cos\alpha\sin\theta - \sin\alpha\cos\beta) \\
mV\dot{\beta} = Y - mV(-p\sin\alpha + r\cos\alpha) \\
mV\dot{\alpha} = -T\sin\alpha - L + mVq + mg(\sin\alpha\sin\theta + \cos\alpha\cos\theta) \\
\dot{\phi} = p + (r\cos\phi + q\sin\phi)\tan\theta \\
\dot{\theta} = q\cos\phi - r\sin\phi \\
\dot{\psi} = \frac{1}{\cos\theta}(r\cos\phi + q\sin\phi) \\
\dot{p} = (c_1 r + c_2 p)q + c_3\bar{L} + c_4 N \\
\dot{q} = c_5 pr - c_6(p^2 - r^2) + c_7 M \\
\dot{r} = (c_8 p - c_2 r)q + c_4\bar{L} + c_9 N \\
\dot{x}_g = u\cos\theta\cos\psi + v(\sin\phi\sin\theta\cos\psi - \cos\phi\sin\psi) \\
\qquad +w(\sin\phi\sin\psi + \cos\phi\sin\theta\cos\psi) \\
\dot{y}_g = u\cos\theta\sin\psi + v(\sin\phi\sin\theta\sin\psi + \cos\phi\cos\psi) \\
\qquad +w(-\sin\phi\cos\psi + \cos\phi\sin\theta\sin\psi) \\
\dot{h} = u\sin\theta - v\sin\phi\cos\theta - w\cos\phi\cos\theta
\end{cases}
\tag{1}
$$

Where:

$$
\begin{bmatrix} u \\ v \\ w \end{bmatrix} = S_{\alpha\beta}^{T} \begin{bmatrix} V \\ 0 \\ 0 \end{bmatrix}_{\text{wind}} = \begin{bmatrix} V\cos\alpha\cos\beta \\ V\sin\beta \\ V\sin\alpha\cos\beta \end{bmatrix} \tag{2}
$$

$$
\begin{aligned}
&c_1 = \frac{(I_y - I_z)I_z - I_{xz}^2}{\Sigma}, c_2 = \frac{(I_x - I_y + I_z)I_{xz}}{\Sigma}, c_3 = \frac{I_z}{\Sigma}, c_4 = \frac{I_{xz}}{\Sigma}, c_5 = \frac{I_z - I_x}{I_y}, \\
&c_6 = \frac{I_{xz}}{I_y}, c_7 = \frac{1}{I_y}, c_8 = \frac{I_x(I_x - I_y) + I_{xz}^2}{\Sigma}, c_9 = \frac{I_x}{\Sigma}, \Sigma = I_x I_z - I_{xz}^2
\end{aligned}
\tag{3}
$$

Within the body coordinate system, u, v, w indicate the UAV's three directional components, Ix, Iy, Iz correspond to the moments of inertia around the three body axes, and Ixz is the product of inertia.

Accordingly, the nonlinear mathematical representation for multiple UAVs is captured by the following generalized system of nonlinear differential equations:

© 2023 The Author(s). | Published by Agro Intelligence Research Press

$$\begin{cases} \dot{x} = f(t, x, u) \\ y = g(t, x, u) \end{cases} \quad (4)$$

In this formulation, t denotes time, x represents the system state, u denotes the control input, and y denotes the output. The collection of state variables—airspeed, angle of attack, sideslip angle, roll angle, pitch angle, heading angle, roll rate, pitch rate, yaw rate, vertical displacement, lateral displacement, and altitude—is expressed as x=[V, α, β, ϕ, θ, ψ, p, q, r, xg, yg, h], while the control variables u=[T, D, Y, L, M, N] respectively denote thrust, drag, side force, rolling moment, pitching moment, and yawing moment. Aerodynamic coefficients determine these control variables.

In the present article, when formation control of a UAV focuses solely on positions and velocities, an inner/outer loop structure can be employed to achieve formation control [43, 44]. The reasoning is that the UAV's trajectory dynamics exhibit time constants that are considerably larger than those of its attitude dynamics. Under this arrangement, the outer loop drives the UAV towards the intended position and velocity, while the inner loop handles attitude tracking. The emphasis of this brief is placed on constructing the outer loop.

At the formation control stage, a UAV may be approximated as a point–mass system, permitting its dynamics to be simplified and characterized by the following equations [45]:

$$\begin{cases} \dot{x}_l = u_l \cos \psi_l \\ \dot{y}_l = u_l \sin \psi_l \\ \dot{\psi}_l = r_l \\ \dot{u}_l = T_l + \vartheta_{T,l} \\ \dot{r}_l = \tau_l + \vartheta_{\tau,l} \end{cases} \quad (5)$$

For i=1,…,n, with $\boldsymbol{pi}$=[xi, yi]T representing the UAV position, ui and ri being the airspeed and yaw angle rate of the UAV, respectively, ψi denoting the yaw angle, Ti representing the thrust force, τi being the yawing moment, and nominal disturbances $\boldsymbol{\vartheta} i$=[$\vartheta T,i$, $\vartheta \tau,i$]T=[ΔTi+du,i, $\Delta \tau i$+dr,i]T. The thrust force error and yawing moment error arising from the actuator fault are captured by ΔTi and $\Delta \tau i$, respectively. External disturbances are represented by du, and dr,. As a standard assumption, for any time k, the nominal disturbance $\boldsymbol{\vartheta} i$ remains bounded such that $|(k)| \leq \vartheta 0$, with $\vartheta 0$ being a positive constant.

Several practical lemmas are stated below:

Lemma 1 ([46]): For any prescribed continuous function $f(x)$ fulfilling $f(0)=0$ on a compact set Ωx, the use of continuous function separation and RBFNN approximation methods enables $f(x)$ to be ultimately expressed as

$$f(x) = AS(x) + \varepsilon(x), \forall x \in \Omega_x \quad (6)$$

Where the approximation error (x) meets:

© 2023 The Author(s). | Published by Agro Intelligence Research Press

$$|\varepsilon(x)| \leq \bar{\varepsilon}.\quad S(x) = (S_1(x), S_2(x), \ldots, S_l(x))^T \tag{7}$$

Denotes the Gaussian basis function vector where:

$$S_j(x) = \exp\left(-\frac{(x-e)^T(x-e)}{2\sigma^2}\right), \tag{8}$$

j=1,2,…,l, with ϱ and σ being the center and width of the Gaussian basis function $Sj(x)$, respectively. A stands for the optimal weight matrix, m gives the dimensionality of the state vector x, and n indicates the NN node count.

$$A = \begin{bmatrix} \omega_{11} & \omega_{12} & \cdots & \omega_{1m} \\ \omega_{21} & \omega_{22} & \cdots & \omega_{2m} \\ \vdots & \vdots & \ddots & \vdots \\ \omega_{n1} & \omega_{n2} & \cdots & \omega_{nm} \end{bmatrix} \tag{9}$$

Lemma 2 ([47]): For any variable ϱ along with a positive continuous function (t) where t>0, the following relationship is established:

$$|\varrho| - \varrho \tanh\frac{\varrho}{\xi(t)} \leq \varphi\xi(t), \tag{10}$$

With the constant φ>0.

Lemma 3: For ∀a, b ≥0, and p, q>0 meeting 1/p+1/q=1, the inequality $\mathrm{ab} \leq \frac{\mathrm{ap}}{\mathrm{p}} + \frac{\mathrm{bq}}{\mathrm{q}}$ is valid.

Description of the communication topologies

Graph theory serves to model the communication structure of the UAV formation system. Let $\mathcal{G}$=($\mathcal{V}$, $\mathcal{E}$, $\mathcal{A}$) be a weighted directed graph, where $\mathcal{V}$={vi, i=1,…,n} is the vertex set, $\mathcal{E}\subseteq\mathcal{V}\times\mathcal{V}$ is the edge set, and $\mathcal{A}$=[ai,j]∈$\mathbb{R}n\times n$ constitutes the weighted adjacency matrix of $\mathcal{G}$, whose entries {ai,j} are non-negative, with ai,j=1 if (i,j)∈$\mathcal{E}$ and $i\neq j$, and ai,j=0 otherwise, implying the i-th UAV acquires information from the j-th UAV whenever (i,j)∈$\mathcal{E}$. The neighbor set of the j-th UAV is given by nj={i∈$\mathcal{V}$|(i,j)∈$\mathcal{E}$}. The Laplacian matrix of $\mathcal{G}$ is defined as $\mathcal{L}$=$\mathcal{D}$−$\mathcal{A}$, in which the diagonal matrix $\mathcal{D}$=($d^{in}1$,…,$d^{in}n$), $\mathrm{d}_{\mathrm{i}}^{\mathrm{im}} = \sum_{\mathrm{j}=1}^{\mathrm{n}} \mathrm{ai,j}$ corresponds to the indegree of vertex i. The discussion herein assumes a fixed, strongly connected graph during control, guaranteeing a path linking any two distinct vertices.

© 2023 The Author(s). | Published by Agro Intelligence Research Press

Additionally, a fictitious leader is introduced as vertex 0, possessing the command consensus reference trajectory yd, and communication is set up between vertex 0 and at least one UAV. Hence, the directed graph is expanded to $\bar{\mathcal{G}} = \left(\mathcal{V} \cup \{0\}, \bar{\mathcal{E}}, \bar{\mathcal{A}}\right)$, where $\bar{\mathcal{E}}$ and $\bar{\mathcal{A}}$ denote the extended edge set and extended weighted adjacency matrix, respectively.

Main Results

In this section, the event-triggered mode is first described. The tracking controller for the reference trajectory is constructed independently along the x and y directions, incorporating predefined performance constraints. Leveraging the established event-triggered mechanism, the yaw angle and velocity loops are subsequently regulated via the aperiodic sampling mode. The flight control scheme for attitude stabilization of every agent within the formation is then laid out.

Event-triggering mode

The event-triggering mode is formulated from the following control input sampling errors:

$$\varsigma_r(t) = \tau_{d,i}(t) - \bar{\tau}_{d,i}, \quad (11)$$

$$\varsigma_u(t) = T_{d,i}(t) - \bar{T}_{d,i}, \quad (12)$$

With (t) and $\varsigma(t)$ signifying the sampling errors of the control inputs $\tau d,i(t)$ and $Td,i(t)$, corresponding to the yaw angle loop and velocity loop, respectively. Taking ςr, ϕr, γr, $\bar{\gamma} r$ as positive constants fulfilling $\bar{\gamma} r > \gamma r + \phi r$, the triggering rule for $\tau d,(t)$ is then given by:

$$\begin{cases} \bar{\tau}_{d,i} = \tau_{d,i}(t_k), t \in [t_k, t_{k+1}) \\ t_{k+1} = \inf\{t \in R, |\varsigma(t)| \geq \gamma_r \tanh|\tau_{d,i}| + \phi_r\}, \end{cases} \quad (13)$$

tk marks the update instant, k being a positive integer. It follows that $\bar{\tau} d$, stays constant over $t \in [tk, tk+1)$ and switches from $\tau d,i(tk)$ to $\tau d,i(tk+1)$ at $t=tk+1$. The set $\{tk, k \in \mathbb{N}\}$ collects the triggering instants, with the initial event at $t0=0$. The duration $tk-tk-1$ between successive instants is referred to as the inter-event time; note that the sampling error resets to 0 at every triggering instant. In a parallel manner, by setting ςu, ϕu, γu, $\bar{\gamma} u$ as positive constants satisfying $\bar{\gamma} u > \gamma u + \phi u$, and with $(t)=Td,i(t)-\bar{T} d,i$, the triggering rule for $Td,i(t)$ is expressed as

$$\begin{cases} \bar{T}_{d,i} = T_{d,i}(t_k), t \in [t_k, t_{k+1}) \\ t_{k+1} = \inf\{t \in R, |\varsigma(t)| \geq \gamma_u \tanh|T_{d,i}| + \phi_u\}, \end{cases} \quad (14)$$

Likewise, $\bar{T} d$, remains unchanged over $t \in [tk, tk+1)$ and is updated from $Td,i(tk)$ to $Td,i(tk+1)$ at $t=tk+1$.

Trajectory-tracking controller design with predefined performance constraints

© 2023 The Author(s). | Published by Agro Intelligence Research Press

A formation-tracking controller for the UAVs is constructed here, meeting the performance bounds deduced from a Lyapunov candidate function, under the assumption that formation member i neighbors member j. The controller aims to steer the position pi toward the target vector $\boldsymbol{pi,d}=[xi,d,yi,d]^T=[xj,yj]^T+[\Delta xi,j,\Delta yi,j]^T$.

As illustrated in **Figure 1**:

$$\begin{bmatrix} e_{x,t} \\ e_{y,t} \end{bmatrix} = \begin{bmatrix} \cos\psi_{ij,d} & -\sin\psi_{ij,d} \\ \sin\psi_{ij,d} & \cos\psi_{ij,d} \end{bmatrix}^T (p_t - p_{t,d}) \quad (15)$$

Where $\psi ij,=\text{atan2}(y'j(t)+\Delta x'i,j(t), x'j+\Delta y'i,j)\in[-\pi, \pi]$.

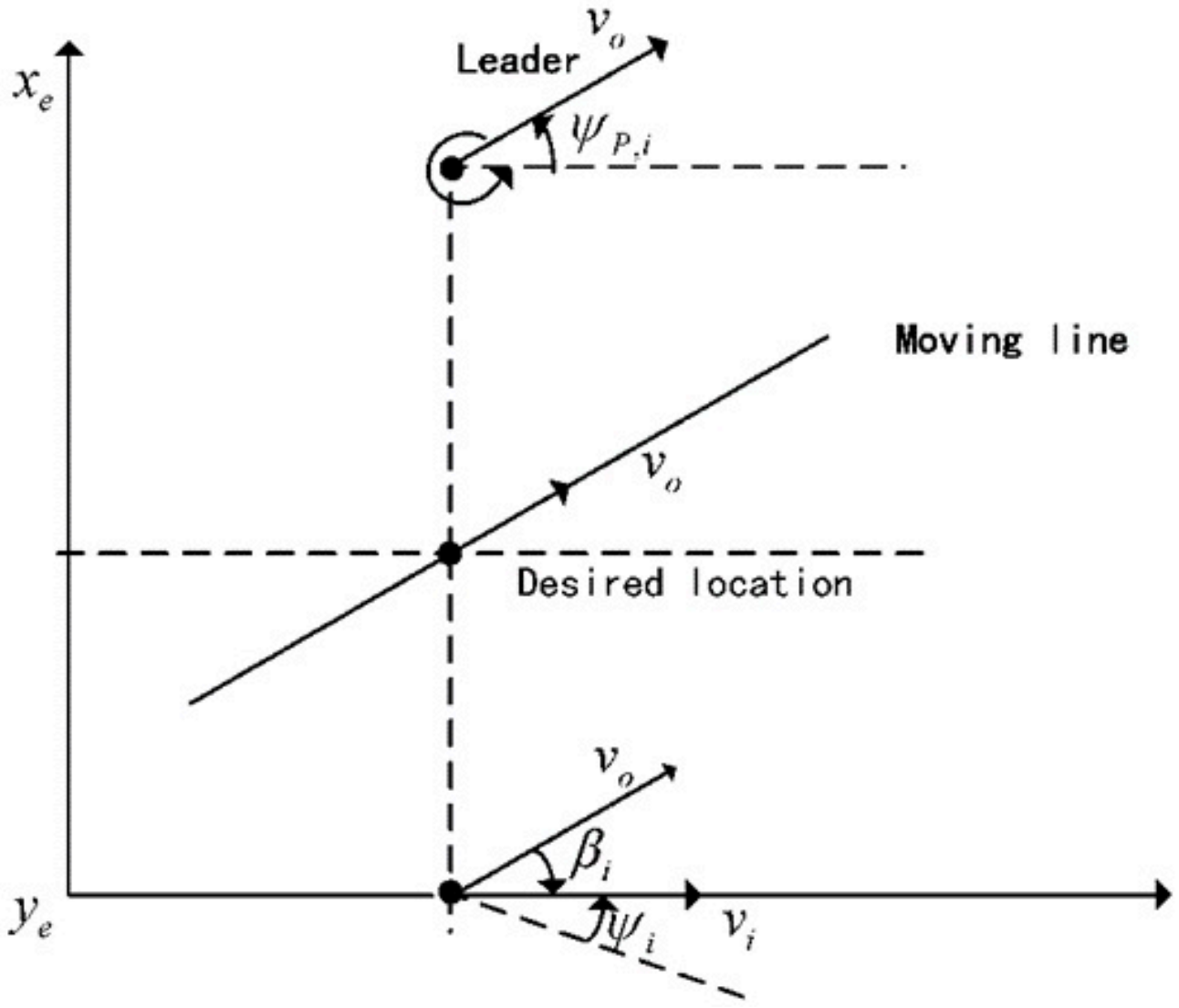

Figure 1. Schematic diagram of geometric relationship.

It is straightforward to derive the time derivative of ey, as:

© 2023 The Author(s). | Published by Agro Intelligence Research Press

$$\dot{e}_{y,i} = u_i \sin\left(\psi_i - \psi_{ij,d}\right) \quad (16)$$

Using the vector field guidance law, the desired yaw angle ψd, is formulated as:

$$\psi_{d,i} = \psi_{ij,d} + \arcsin\left(-\frac{k_y b_{y,i}^2}{2u_i \pi e_{y,i}} \sin\left(\frac{\pi e_{y,i}^2}{b_{y,i}^2}\right) + \frac{\dot{b}_{y,i}}{u_i b_{y,i}} e_{y,i}\right) \quad (17)$$

With ky>0 serving as the guidance law parameter.

From **Figure 1**, the time derivative of follows as:

$$\dot{e}_{x,i} = u_i \cos\beta_i - u_j \quad (18)$$

Then the desired velocity is formulated as:

$$u_{d,i} = \frac{1}{\cos\beta_i}\left(-\frac{k_v b_{x,i}^2}{2\pi e_{x,i}} \sin\left(\frac{\pi e_{x,i}^2}{b_{x,i}^2}\right) + \frac{\dot{b}_{x,i}}{b_{x,i}} e_{x,i} + u_j\right) \quad (19)$$

With $\beta i=\psi ij,d-\psi i$, where the predefined performance constraints are enforced as $||ex,i||\leq bx,i$, $||ey,i||\leq by,i$, by,i and bx,i corresponding to the upper bounds on ey,i and ex,i, respectively. A thorough analysis is subsequently performed using the Lyapunov candidate function, as described in (A1)-(A4).

Yaw angle controller design

The angular deviation for any formation member is specified as:

$$e_{\psi,i} = \psi_i - \psi_{d,i} \quad (20)$$

A command filter is brought in to suppress the differential explosion phenomenon linked to $\psi d,,$, given by:

$$\begin{aligned} \dot{X}_1 &= X_2 \\ \dot{X}_2 &= -2\zeta\omega_n X_2 - \omega_n{}^2 (X_1 - \psi_{d,i}) \end{aligned} \quad (21)$$

Within which ζ and ωn act as the filter coefficients, ψd, represents the input signal, $X1$ approximates $\psi d,$, and $X2$ approximates the time derivative of $\psi d,i$, $\widehat{\psi}d,i = X2$.

The filtering discrepancy is quantified as:

© 2023 The Author(s). | Published by Agro Intelligence Research Press

$$\tilde{\dot{\psi}}_{d,t} = \dot{\psi}_{d,t} - \hat{\dot{\psi}}_{d,t} \quad (22)$$

An adaptive mechanism is devised to compensate for this filtering discrepancy, expressed as:

$$\dot{\hat{d}}_{\psi,t} = k_{1,\psi,t}\left(e_{\psi,t} - k_{2,\psi,t}\hat{d}_{\psi,t}\right) \quad (23)$$

Featuring the positive design constants $k1,,, k2,\psi,i$.

The adaptive tracking control law, together with the commanded yaw angular rate, can be constructed as:

$$r_{d,t} = -k_{3,\psi,t}e_{\psi,t} - \hat{d}_{\psi,t} + \hat{\dot{\psi}}_{d,t} \quad (24)$$

Thereafter, the yaw angular rate tracking discrepancy is given by:

$$e_{r,t} = r_t - r_{d,t} \quad (25)$$

A command filter is brought in to suppress the differential explosion phenomenon linked to rd, given by:

$$\begin{aligned} \dot{Y}_1 &= Y_2 \\ \dot{Y}_2 &= -2\zeta\omega_n Y_2 - \omega_n{}^2\left(Y_1 - r_{d,t}\right) \end{aligned} \quad (26)$$

Within which ζ and ωn act as the filter coefficients, rd,i represents the input signal, $Y1$ approximates rd,i, and $Y2$ approximates the time derivative of rd,i, $\widehat{\dot{\psi}}d,i=Y2$.

The filtering discrepancy is quantified as:

$$\tilde{\dot{r}}_{d,t} = \dot{r}_{d,t} - \hat{\dot{r}}_{d,t} \quad (27)$$

Taking the time derivative of the yaw rate tracking discrepancy:

$$\begin{aligned} \dot{e}_{r,t} &= \dot{r}_t - \dot{r}_{d,t} \\ &= \tau_t + \Delta\tau_t + d_{r,t} - \hat{\dot{r}}_{d,t} - \tilde{\dot{r}}_{d,t} \end{aligned} \quad (28)$$

An RBFNN is used to reconstruct the uncertain nonlinear dynamics caused by actuator faults. Consequently:

© 2023 The Author(s). | Published by Agro Intelligence Research Press

$$\begin{aligned}\dot{e}_{r,t} &= r_t + A_{r,t}S_{r,t} + \varepsilon_{r,t} + d_{r,t} - \dot{\widehat{r}}_{d,t} - \dot{\widetilde{r}}_{d,t} \\ &= r_t + A_{r,t}S_{r,t} - \dot{\widehat{r}}_{d,t} + \widetilde{d}_{r,t}\end{aligned} \quad (29)$$

Letting $đr,=\varepsilon r,i+dr,i-r\dot{\tilde{}}\, d,i$ encapsulate the aggregate disturbances. $đr$i is confined within a bound, fulfilling $đr$i. Furthermore, $đr,\leq \underline{d}r,i$. $Ar,=Ar,i-Ar,i$ and $Ar,i\leq r,i$.

An adaptive mechanism is devised to counteract the uncertain nonlinear dynamics attributable to actuator faults, expressed as:

$$\dot{\widehat{A}}_{r,t} = k_{1,r,t}\left(S_{r,t}e_{r,t} - k_{2,r,t}\widehat{A}_{r,t}\right) \quad (30)$$

Featuring the positive design constants $k1,$, and $k2,r,i$.

An additional adaptive mechanism is devised to counteract the aggregate disturbance, expressed as:

$$\dot{\widehat{d}}_{r,t} = k_{3,r,t}\left(e_{r,t} - k_{4,r,t}\widehat{d}_{r,t}\right) \quad (31)$$

Featuring the positive design constants $k3,,$ $k4,r,i$.

The adaptive tracking control law can be constructed as:

$$\tau_{d,t} = -k_{5,r,t}e_{r,t} - \widehat{d}_{r,t} - \widehat{A}_{r,t}S_{r,t} + \dot{\widehat{r}}_{d,t} - \overline{\gamma}_r \tanh\left(\frac{\overline{\gamma}_r e_{r,t}}{\xi_r}\right) \quad (32)$$

Under the event-triggering strategy, it can be deduced from (A9) that:

$$\begin{aligned}\left|\tau_{d,t}(t) - \overline{\tau}_{d,t}\right| &< \gamma_r \tanh\left|\overline{\tau}_{d,t}\right| + \phi_r \\ &< \gamma_r + \phi_r\end{aligned} \quad (33)$$

Over the interval $t\in[tk,tk+1)$, enabling $\overline{\tau}d,i$ to be reformulated as:

$$\overline{\tau}_{d,t} = \tau_{d,t}(t) - \rho_r(t)(\gamma_r + \phi_r), \quad (34)$$

Where:

© 2023 The Author(s). | Published by Agro Intelligence Research Press

$$\rho_r(t) = \frac{\tau_{d,i}(t) - \overline{\tau}_{d,i}}{\gamma_r + \phi_r} \quad (35)$$

Retains continuity and fulfills $|(t)|<1$.

Velocity controller design

The speed deviation for any formation member is specified as:

$$e_{u,1} = u_1 - u_{d,1} \quad (36)$$

A command filter is brought in to suppress the differential explosion phenomenon linked to ud, given by:

$$\begin{aligned} \dot{Z}_1 &= Z_2 \\ \dot{Z}_2 &= -2\zeta\omega_n Z_2 - \omega_n{}^2 (Z_1 - u_{d,1}) \end{aligned} \quad (37)$$

Within which ζ and ωn act as the filter coefficients, ud,i represents the input signal, $Z1$ approximates ud,i, and $Z2$ approximates the time derivative of ud,i, $\widehat{u}d,i=Z2$.

The filtering discrepancy is quantified as:

$$\tilde{\dot{u}}_{d,1} = \dot{u}_{d,1} - \hat{\dot{u}}_{d,1} \quad (38)$$

Taking the time derivative of the speed tracking discrepancy:

$$\begin{aligned} \dot{e}_{u,1} &= \dot{u}_1 - \dot{u}_{d,1} \\ &= T_1 + \Delta T_1 + d_{u,1} - \hat{\dot{u}}_{d,1} - \tilde{\dot{u}}_{d,1} \end{aligned} \quad (39)$$

An RBFNN is used to reconstruct the uncertain nonlinear dynamics caused by actuator faults. Consequently:

$$\begin{aligned} \dot{e}_{u,1} &= u_1 + A_{u,1}S_{u,1} + \varepsilon_{u,1} + d_{u,1} - \hat{\dot{u}}_{d,1} - \tilde{\dot{u}}_{d,1} \\ &= u_1 + A_{u,1}S_{u,1} - \hat{\dot{u}}_{d,1} + \tilde{d}_{u,1} \end{aligned} \quad (40)$$

Letting $đu,=\varepsilon u,i+du,i-u\tilde{\cdot}\, d,i$ encapsulate the aggregate disturbances. $đu$ is confined within a bound, fulfilling $đu$i. Furthermore, $đu,\leq \underline{d}u,i$. $Au,=Au,i-Au,i$ and $Au,i\leq u,i$.An adaptive mechanism is devised to counteract the uncertain nonlinear dynamics attributable to actuator faults, expressed as:

© 2023 The Author(s). | Published by Agro Intelligence Research Press

$$\dot{\widehat{A}}_{u,t} = k_{1,u,t}\left(S_{u,t}e_{u,t} - k_{2,u,t}\widehat{A}_{u,t}\right) \quad (41)$$

Featuring the positive design constants $k1$,, and $k2,u,i$.

An additional adaptive mechanism is devised to counteract the aggregate disturbance, expressed as:

$$\dot{\widehat{d}}_{u,t} = k_{3,u,t}\left(e_{u,t} - k_{4,u,t}\widehat{d}_{u,t}\right) \quad (42)$$

Featuring the positive design constants $k3$,,, $k4,u,i$.

The adaptive tracking control law can be constructed as:

$$T_{d,t} = -k_{5,u,t}e_{u,t} - \widehat{d}_{u,t} - \widehat{A}_{u,t}S_{u,t} + \dot{\widehat{u}}_{d,t} - \overline{\gamma}_u \tanh\left(\frac{\overline{\gamma}_u e_{u,t}}{\zeta_u}\right) \quad (43)$$

Under the event-triggered mechanism, it can be deduced from (A9) that:

$$\begin{aligned}\left|T_{d,t}(t) - \overline{T}_{d,t}\right| &< \gamma_u \tanh\left|\overline{T}_{d,t}\right| + \phi_u \\ &< \gamma_u + \phi_u\end{aligned} \quad (44)$$

Over the interval $t\in[Tk,Tk+1)$, enabling $\overline{\mathrm{T}}d,i$ to be reformulated as:

$$\overline{T}_{d,t} = T_{d,t}(t) - \rho_u(t)(\gamma_u + \phi_u), \quad (45)$$

Where:

$$\rho_u(t) = \frac{T_{d,i}(t) - \overline{T}_{d,i}}{\gamma_u + \phi_u} \quad (46)$$

Retains continuity and fulfills $|(t)|<1$.

Zeno behavior analysis

This subsection evaluates the practicability of the suggested event-triggering strategy by confirming that Zeno behavior cannot occur. Focusing on the yaw angle loop triggering rule, setting $(t)=\tau d,i(t)-d,i$, yields:

© 2023 The Author(s). | Published by Agro Intelligence Research Press

$$\dot{\varsigma}_u(t) = \dot{\tau}_{d,1}(t) - \dot{\bar{\tau}}_{d,1}. \quad (47)$$

Because d, stays unchanged throughout $t \in [tk, tk+1)$, it becomes evident that:

$$\dot{\varsigma}_u(t) = \dot{\tau}_{d,1}(t), \quad (48)$$

Which directly leads to $\dot{\varsigma}(t) \leq |\dot{\tau} d,i(t)|$.

Referring to **Eq. 32**, the expression of $\dot{\tau} d,(t)$ becomes:

$$\dot{\tau}_{d,1}(t) = -k_{5,r,1}\dot{e}_{r,1} - \dot{\hat{d}}_{r,1} - \dot{\hat{A}}_{r,1}\dot{S}_{r,1} + \dot{\hat{\dot{r}}}_{d,1} - \frac{\bar{\gamma}_r^2\left(\dot{e}_{r,1}\zeta_r + e_{r,1}\dot{\zeta}_r\right)}{\zeta_r^2 \cosh^2 \frac{\gamma_r e_{r,i}}{\zeta_r}}. \quad (49)$$

One can readily see that $\dot{\tau} d,(t)$ remains both smooth and confined within limits:

$$|\dot{\tau}_{d,1}(t)| \leq \Gamma, \quad (50)$$

Holding for some constant Γ>0.

From this, it follows that:

$$\begin{aligned} \int_{T_k}^{T_{k+1}} \dot{\varsigma}_u(t)\, dt &= \varsigma_u(T_{k+1}) - \varsigma_u(T_k) \\ &= \gamma \tanh\left(|\bar{\tau}_{d,1}|\right) + \gamma_r - 0 \\ &\leq \Gamma\,(T_{k+1} - T_k). \end{aligned} \quad (51)$$

Equivalently:

$$T_{k+1} - T_k \geq \frac{\gamma \tanh\left(|\bar{\tau}_{d,1}|\right) + \gamma_r}{\Gamma} \geq \frac{\gamma_r}{\Gamma}, \quad (52)$$

This verifies that the yaw angle loop triggering rule completely averts Zeno behavior.

Through an analogous reasoning process, the boundedness of $\dot{T} d,(t)$ for the velocity loop can be similarly confirmed, yielding the limit $|\dot{T} d,i(t)| \leq \Xi$ with Ξ>0. As a result, a minimum permissible interval $T_{k+1} - Tk$ for the velocity loop exists, stated as:

© 2023 The Author(s). | Published by Agro Intelligence Research Press

$$T_{k+1} - T_k \geq \frac{\gamma \tanh\left(|\overline{T}_{d,l}|\right) + \gamma_r}{\Xi} \geq \frac{\gamma_v}{\Xi}, \quad (53)$$

Accordingly, Zeno's behavior is categorically ruled out, and the feasibility verification is accomplished.

Remark 1: In practice, the holistic flight control architecture for each formation agent includes the pitch angle regulation law, the pitch rate regulation law, the longitudinal angle-of-attack controller, and the lateral-loop controller that stabilizes the attitude dynamics. These control components, while omitted from detailed exposition in this paper, form an integral part of each aircraft's onboard control system, essentially following the framework of Lungu [17], and are treated as a conventional design template for fixed-wing aircraft.

Simulation Results

A simulation configuration comprising a single leader and three followers is built to validate the performance of the formation-tracking controller proposed in this study.

Four UAVs are instantiated for simulation verification; employing the leader–follower framework, one leader (AL) and three followers (AF1, AF2, and AF3) are chosen. The communication topology interconnecting the UAVs is depicted in **Figure 2**.

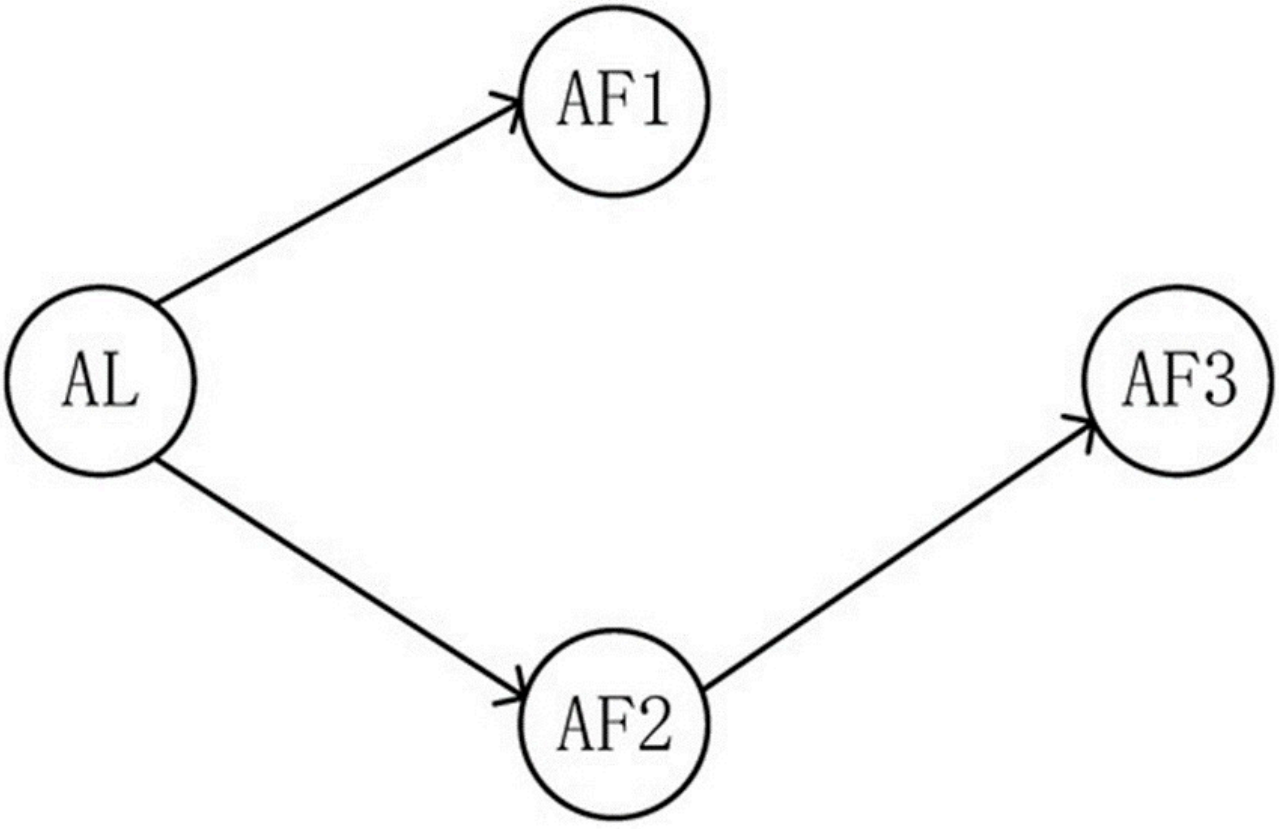

Figure 2. Communication topology diagram among UAV formations.

© 2023 The Author(s). | Published by Agro Intelligence Research Press

Drawing from the directed communication topology graph among UAVs, namely **Figure 2**, the Laplacian matrix is determined as:

$$\boldsymbol{L}=\begin{bmatrix}0 & 0 & 0 & 0\\ -1 & 1 & 0 & 0\\ -1 & 0 & 1 & 0\\ -1 & 0 & 0 & 1\end{bmatrix} \tag{54}$$

The simulation setup adopts the following assumptions:

The external disturbances are specified as:

$$\begin{cases} d_u = 0.3\sin\left(0.1t+\frac{\pi}{6}\right)\\ d_r = 0.2\sin\left(0.2t+\frac{\pi}{4}\right)\end{cases} \tag{55}$$

The faulty control inputs are modeled as:

$$\begin{cases} T = T_c + p_u\,(t-T_c)\left[(l_u\,(t)-1)T_c+\overline{T}_c\right]\\ \tau = \tau_c + p_r\,(t-T_c)\left[(l_r\,(t)-1)\tau_c+\overline{\tau}_c\right]\end{cases} \tag{56}$$

Within which $\boldsymbol{u}=[T,\tau]^{\mathrm{T}}$ indicates the actual control inputs; $\boldsymbol{u}c=[Tc,\tau c]^{\mathrm{T}}$ are the control inputs produced by the controller; $\boldsymbol{l}=[lu(t),lr(t)]^{\mathrm{T}}$ characterizes the actuator effectiveness coefficient, obeying $0<li(t)<1(i=u,r)$; $c=[c,c]\mathrm{T}$ designates the unknown inputs under fault conditions; and $\boldsymbol{p}=[pu,pr]^{\mathrm{T}}$ constitutes the fault distribution with $pi(t-Tc)(i=u,r)$, defined by

$$p_l\,(t-T_c)=\begin{cases}0 & \text{if } t<T_c\\ 1-e^{-a(t-T_c)} & \text{if } t\geq T_c\end{cases} \tag{57}$$

Where $a>0$, and Tc marks the occurrence instant of the actuator fault.

Utilizing the controller designs outlined in Section 3, the subsequent control parameters are adopted:

The followers' guidance law parameters are taken as $kyi=1.01$, $vi=1.1$, $i=1,2,3$. The yaw controller parameters are specified as $k\psi 1=10$, $\psi 2=0.01$, $k\psi 3=1$, $kr1=1$, $kr2=0.01$, $kr3=3$. The velocity controller parameters are set as $kv1=1$, $v2=0.01$, $kv3=0.1$. Meanwhile, for the neural network configuration, the node count equals 301, and the Gaussian function

© 2023 The Author(s). | Published by Agro Intelligence Research Press

width is 0.1. The adaptive law parameters are fixed as $kw\psi$=8, wv=18. The error bound constraints are defined as xb=2+40e−0.2t, b=2+40e−0.2t.

Furthermore, throughout this simulation, the leader's desired time-varying trajectory is given by:

$$\begin{aligned} x_d &= 20\sin(t/10) + 20\cos(t/5) \\ y_d &= 20t \\ V_{xd} &= 2\cos(t/10) - 4\sin(t/5) \\ V_{yd} &= 20 \\ \psi_d &= a\tan 2\left(V_{yd}, V_{xd}\right) \\ V_d &= \sqrt{V_{xd}^2 + V_{yd}^2} \end{aligned} \tag{58}$$

Each follower's initial condition, along with its desired relative position with respect to the leader, is presented in **Table 1**.

Table 1. Initial states of all UAVs.

UAV (1,2,3)	Initial state [$x0(m)y0(m)\psi 0(\mathrm{rad}/s)v0m/s\gamma 0(\mathrm{rad})]T$	Desired position with the leader [$xr(m)yr(m)]T$
$P1$	[−15.5−26.9001]T	[−40−40]T
$P2$	[−16.550π/601]T	[−40−40]T
$P3$	[−64.520π/301]T	[−800]T

In this context, the unknown disturbance acting on each follower is assigned as ψid=0.001sin(t/10) and vid=0.02sin(t/10).

Within this work, the sampling step size is chosen as h=0.01 s, and the overall sampling duration equals T=100 s. Under the controller introduced in this paper, the four UAVs successfully form a time-varying formation. The formation trajectory-tracking outcome is shown in **Figure 3**. To benchmark the performance of the proposed control algorithm, the fixed-time sliding mode control algorithm based on event-triggered control from Su *et al.* [48] was implemented to achieve formation control. The detailed outcomes appear in **Figure 4**.

© 2023 The Author(s). | Published by Agro Intelligence Research Press

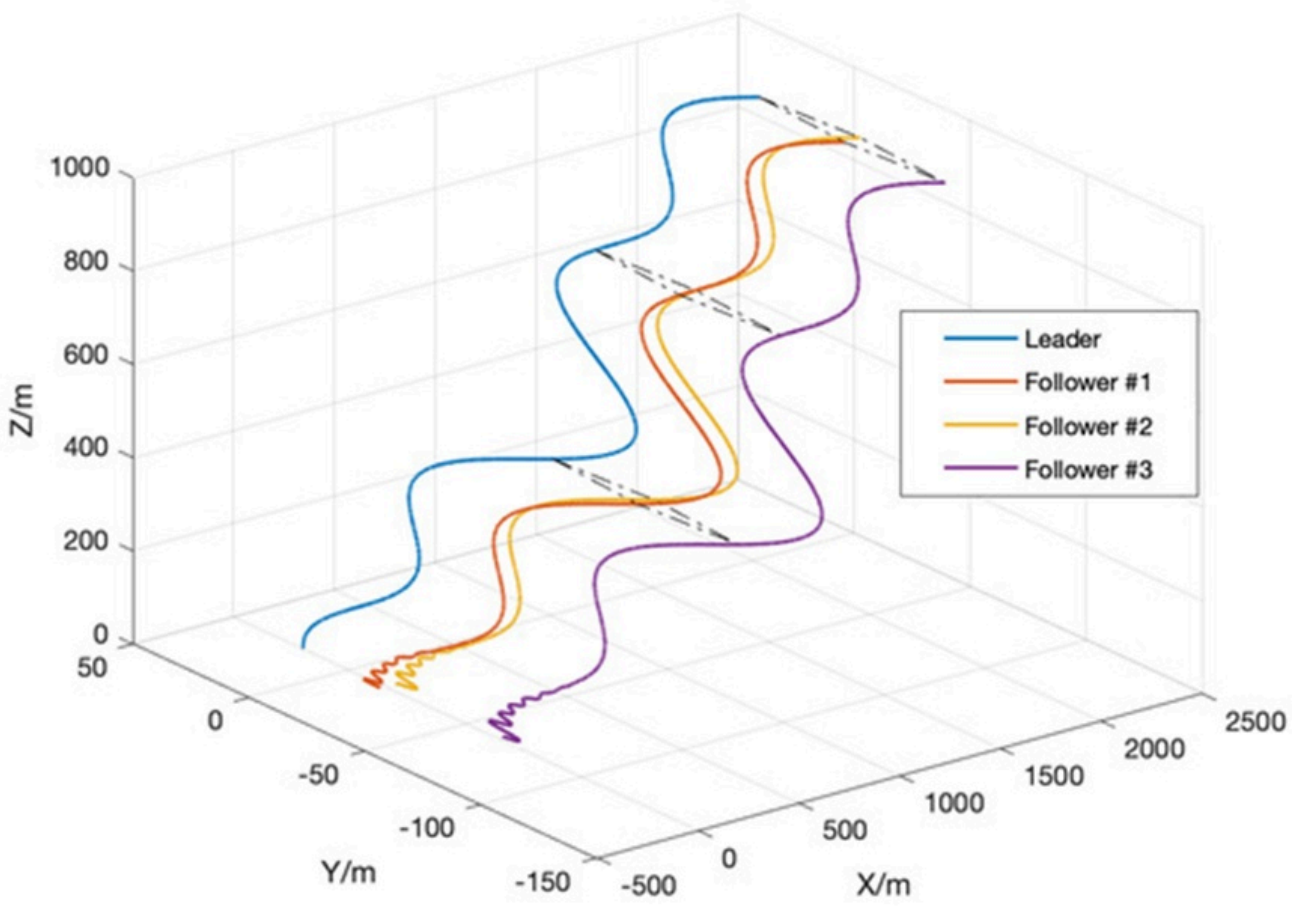

Figure 3. The control algorithm proposed in this paper.

© 2023 The Author(s). | Published by Agro Intelligence Research Press

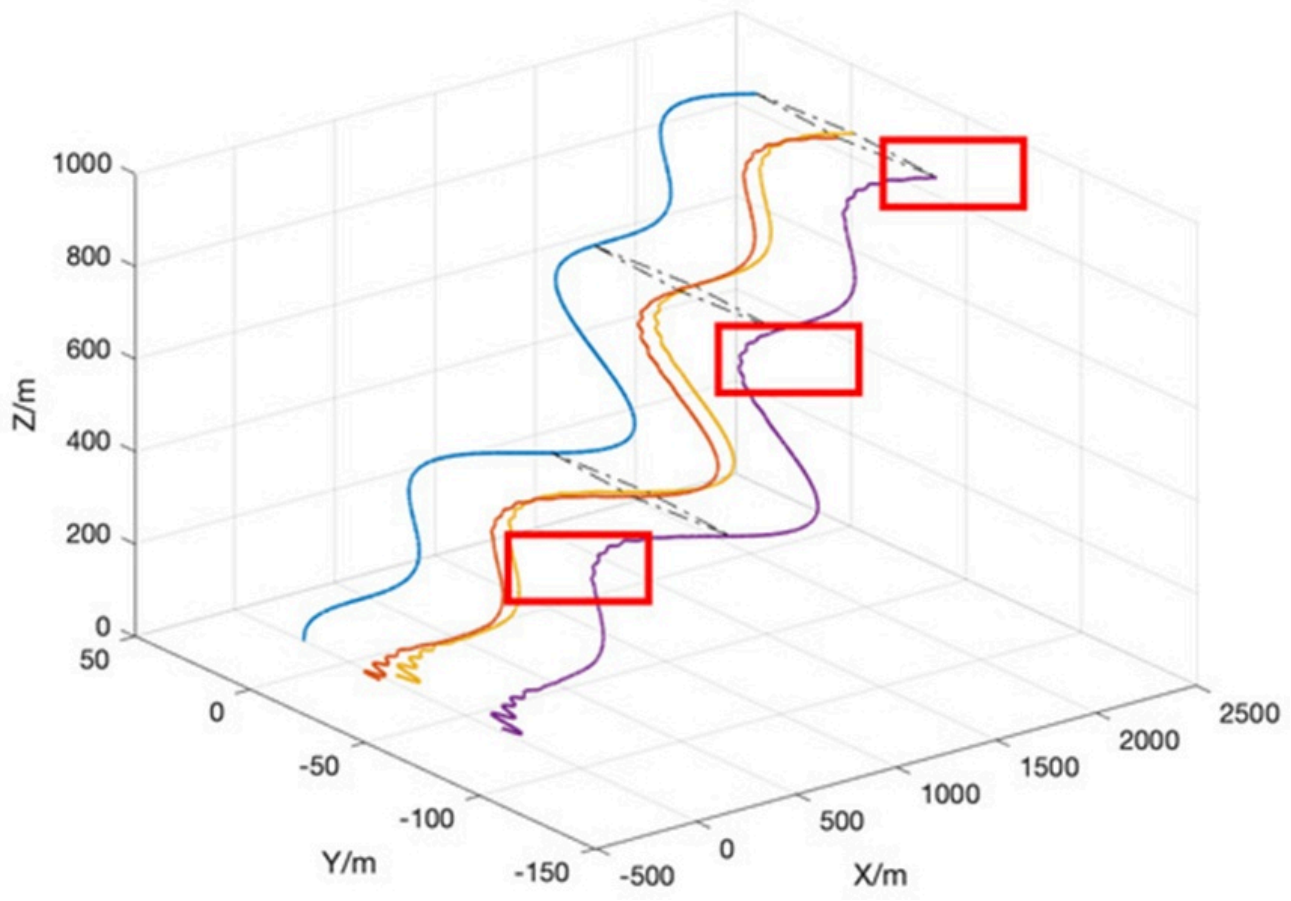

Figure 4. The control algorithm proposed by Su *et al.* [48].

Comparing the simulation results reveals that the control algorithm presented in this work can faithfully estimate and offset disturbances using the RBFNN, thereby successfully mitigating their negative impact on formation control fidelity. By contrast, the technique described by Su *et al.* [48], while capable of partially attenuating disturbances, shows a noticeable drop in controller performance whenever the desired reference trajectory undergoes abrupt changes, leading to oscillatory formation flight paths among follower UAVs, as clearly indicated in the red box in **Figure 4**.

The evolution of tracking error for the followers along the X and Y axes is shown in **Figures 5 and 6**.

© 2023 The Author(s). | Published by Agro Intelligence Research Press

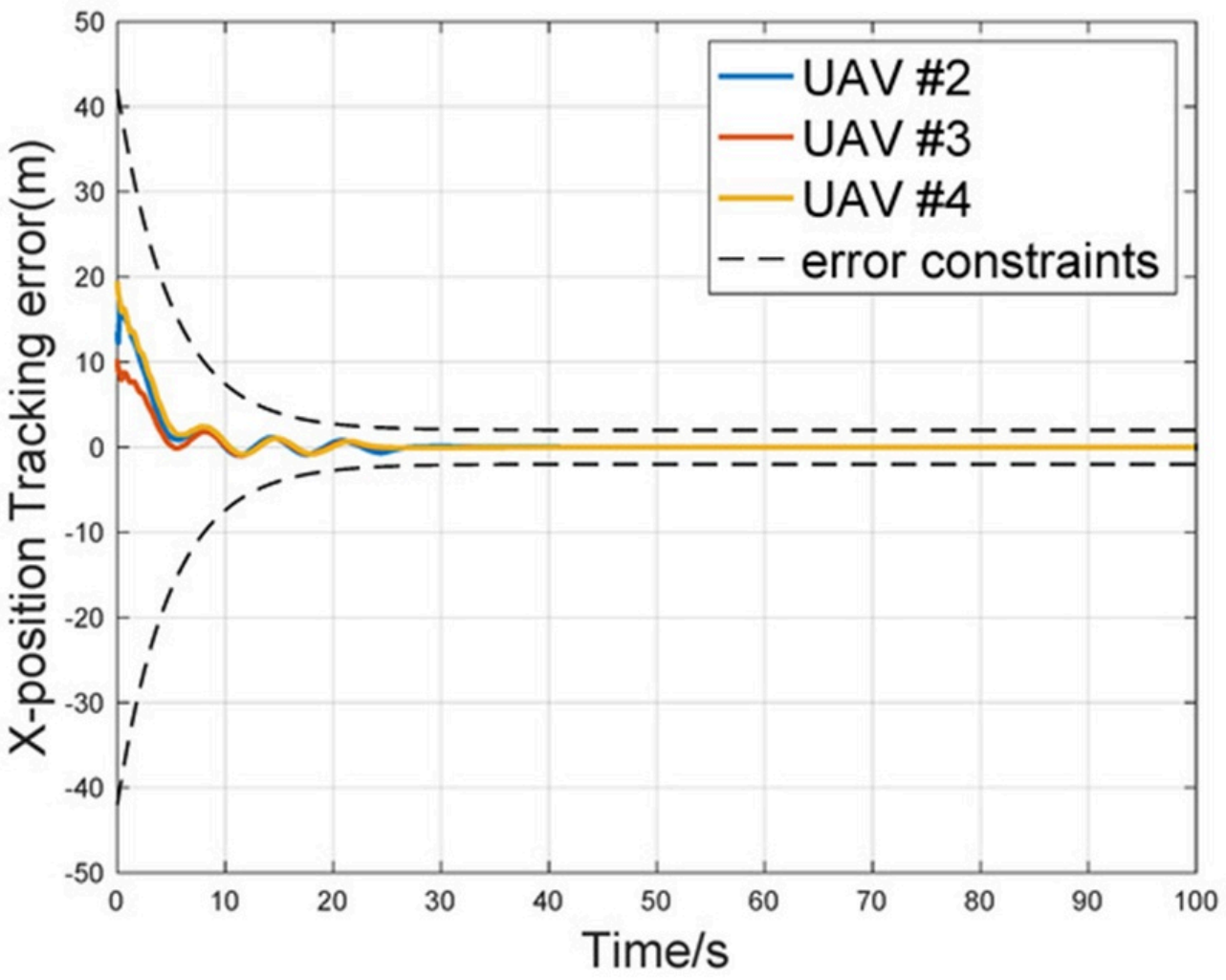

Figure 5. Leader-position tracking error.

© 2023 The Author(s). | Published by Agro Intelligence Research Press

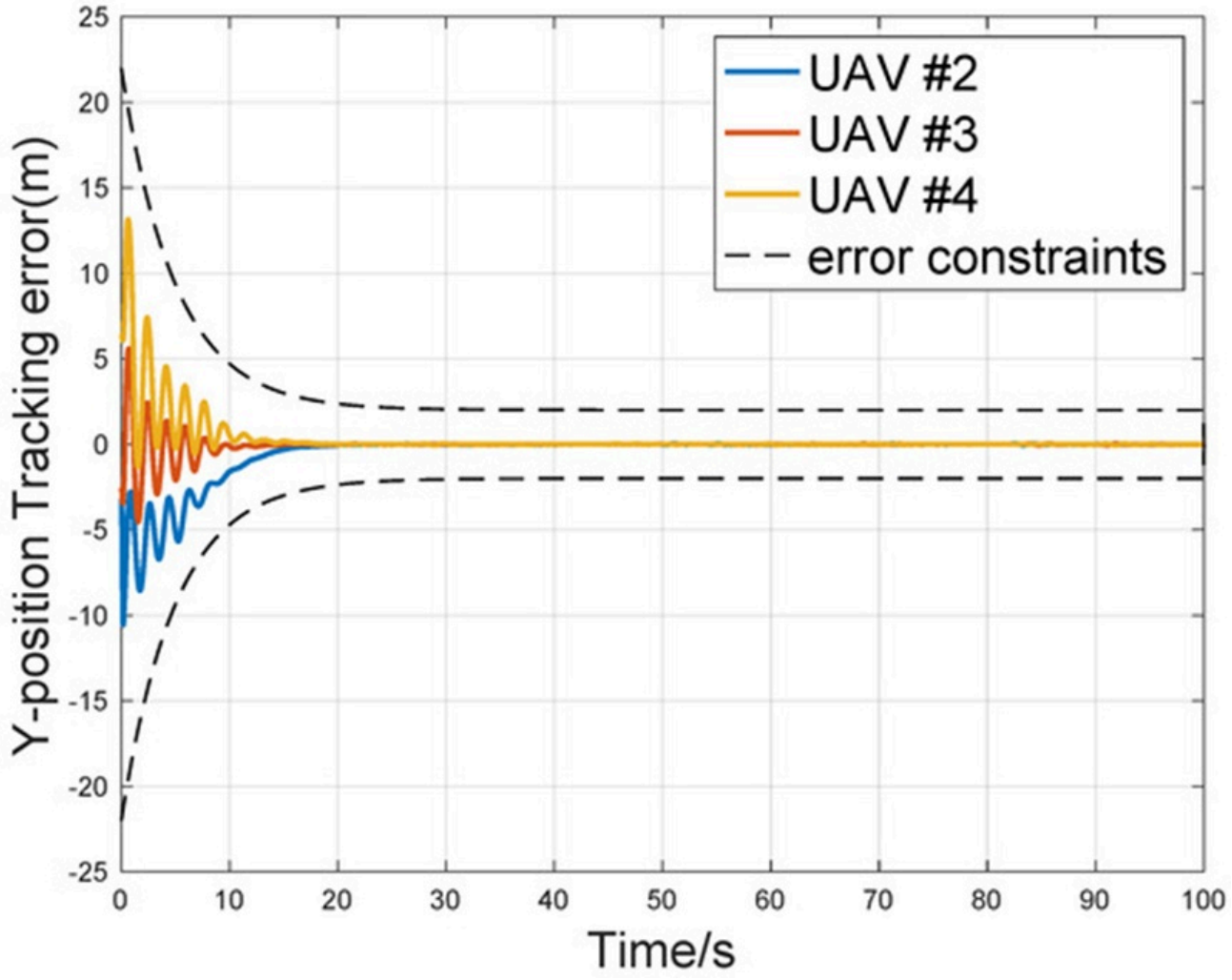

Figure 6. Follower-position tracking error.

The simulation results confirm that the controller formulated in this paper achieves the formation objective even in the presence of external disturbances and actuator faults, with the followers' tracking deviations in both X and Y channels persistently bounded within the prescribed limits. The X-direction tracking error of the followers diminishes to zero around 28 s, whereas the Y-direction tracking error reaches zero at roughly 18 s. Thereafter, the formation maintains steady flight throughout the entire mission.

The temporal variation in flight velocity and heading angle for the leader and followers during formation flight is depicted in **Figures 7 and 8**.

© 2023 The Author(s). | Published by Agro Intelligence Research Press

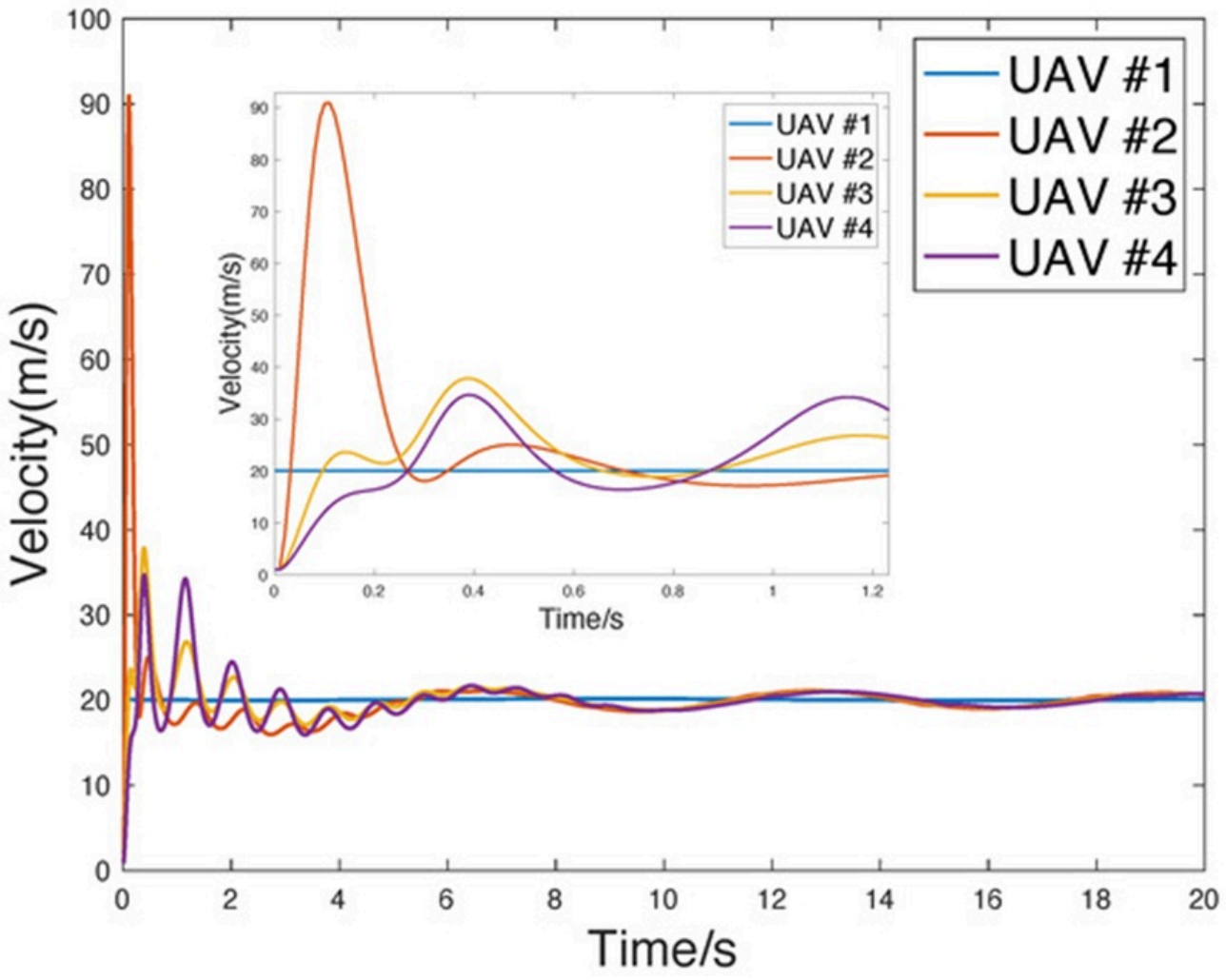

Figure 7. Velocity–time graph.

© 2023 The Author(s). | Published by Agro Intelligence Research Press

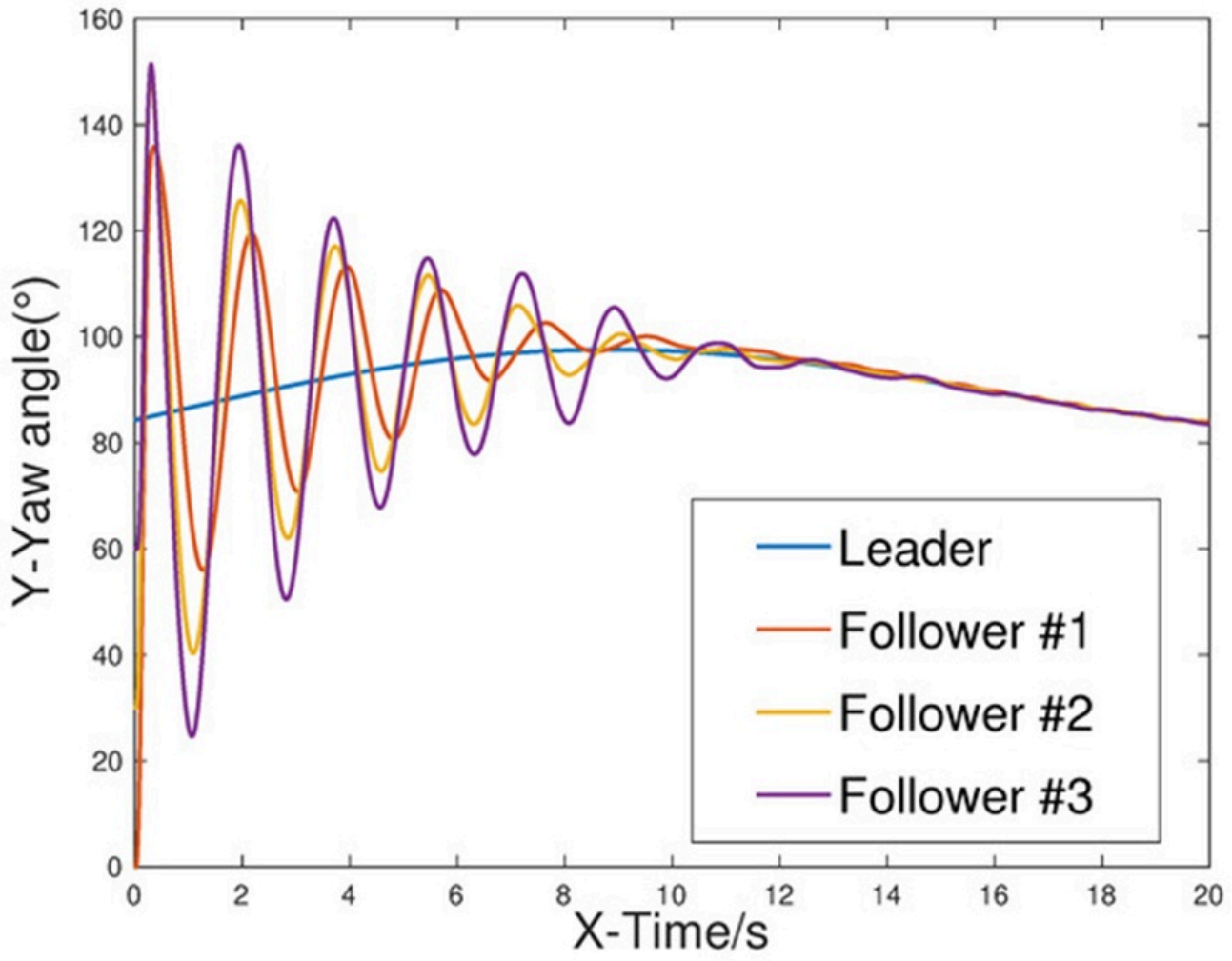

Figure 8. Variation curve of heading angle.

These figures illustrate that the followers' final velocity and heading angle ultimately align with those of the leader, thereby stabilizing the followers at the designated formation positions. Compared with the other UAVs, UAV 2 begins with the largest offset from its intended position. Thus, to rapidly converge on the expected aircraft trajectory, UAV 2 flies at a higher velocity along the desired path during the initial phase. After about 8 s, its velocity converges to the commanded velocity. Its heading angle conforms to the expected heading angle near 14s.

The RBFNN's performance in estimating the external uncertain disturbance is displayed in **Figures 9 and 10**.

© 2023 The Author(s). | Published by Agro Intelligence Research Press

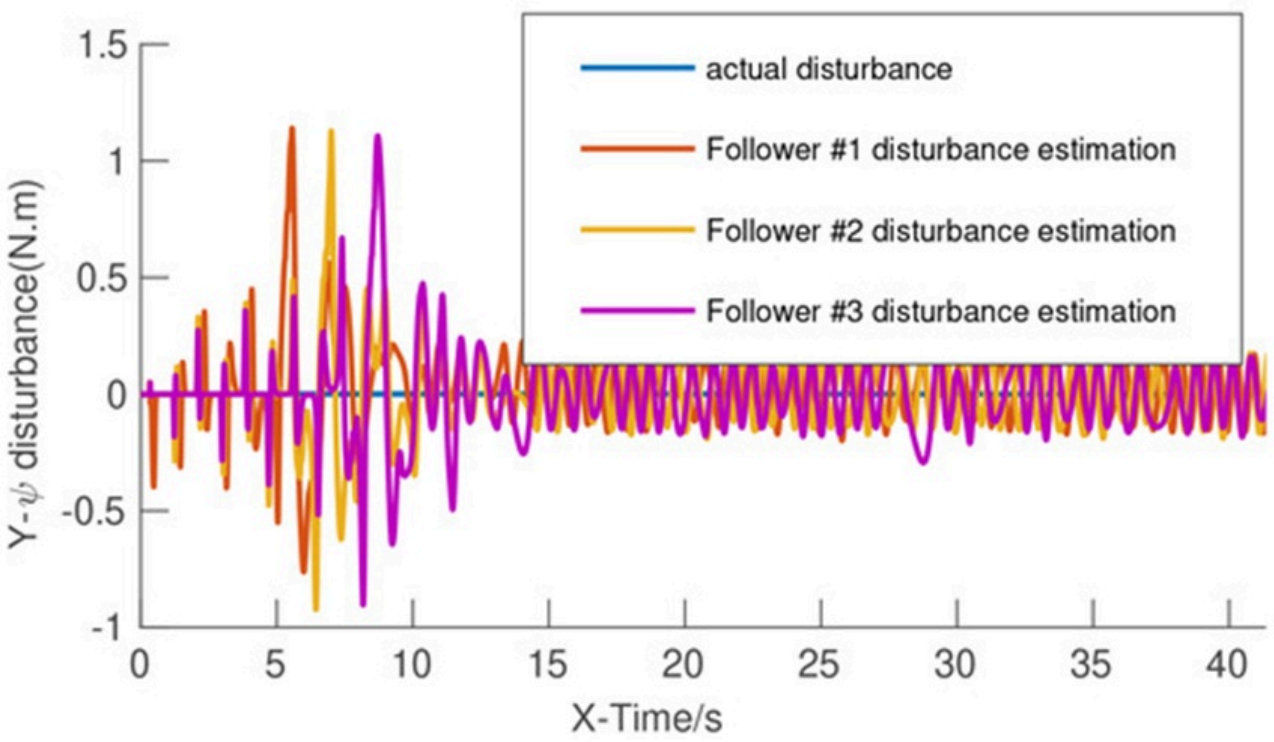

Figure 9. The estimated effect of the disturbance.

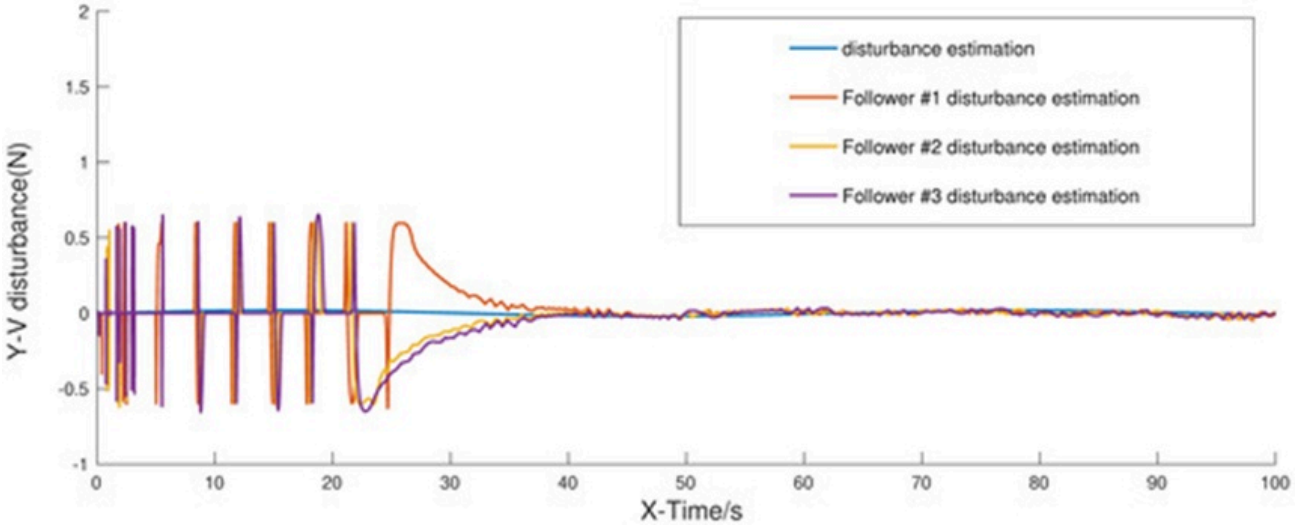

Figure 10. The estimated effect of the disturbance.

The above findings substantiate that the RBFNN neural network advanced in this paper is capable of effectively estimating and neutralizing the external uncertain disturbance.

Figures 11 and 12 plot the variation profiles of the actual output force (torque) delivered by the follower actuators.

© 2023 The Author(s). | Published by Agro Intelligence Research Press

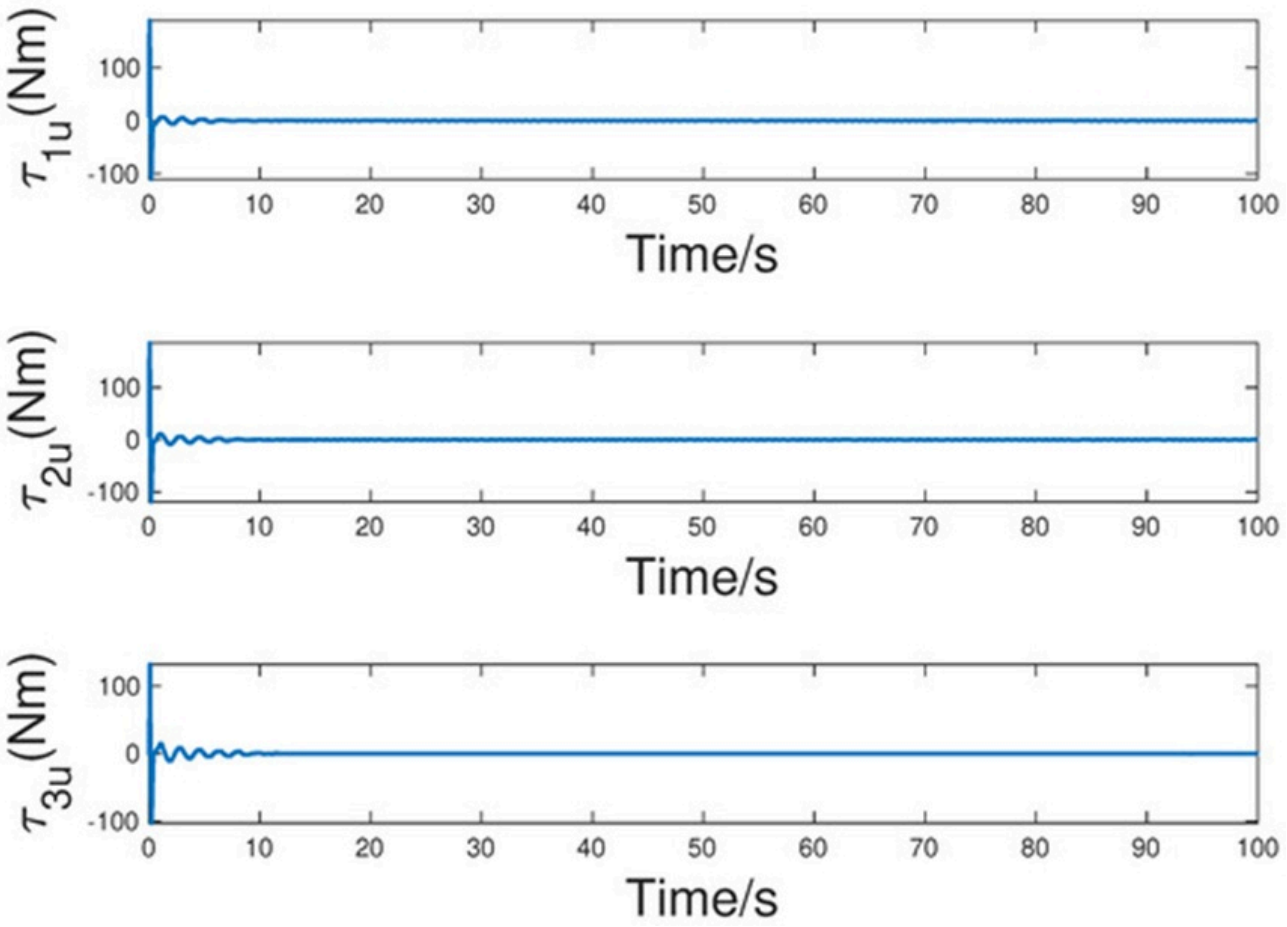

Figure 11. Output force (torque) variation curve of the actuator for the leader.

© 2023 The Author(s). | Published by Agro Intelligence Research Press

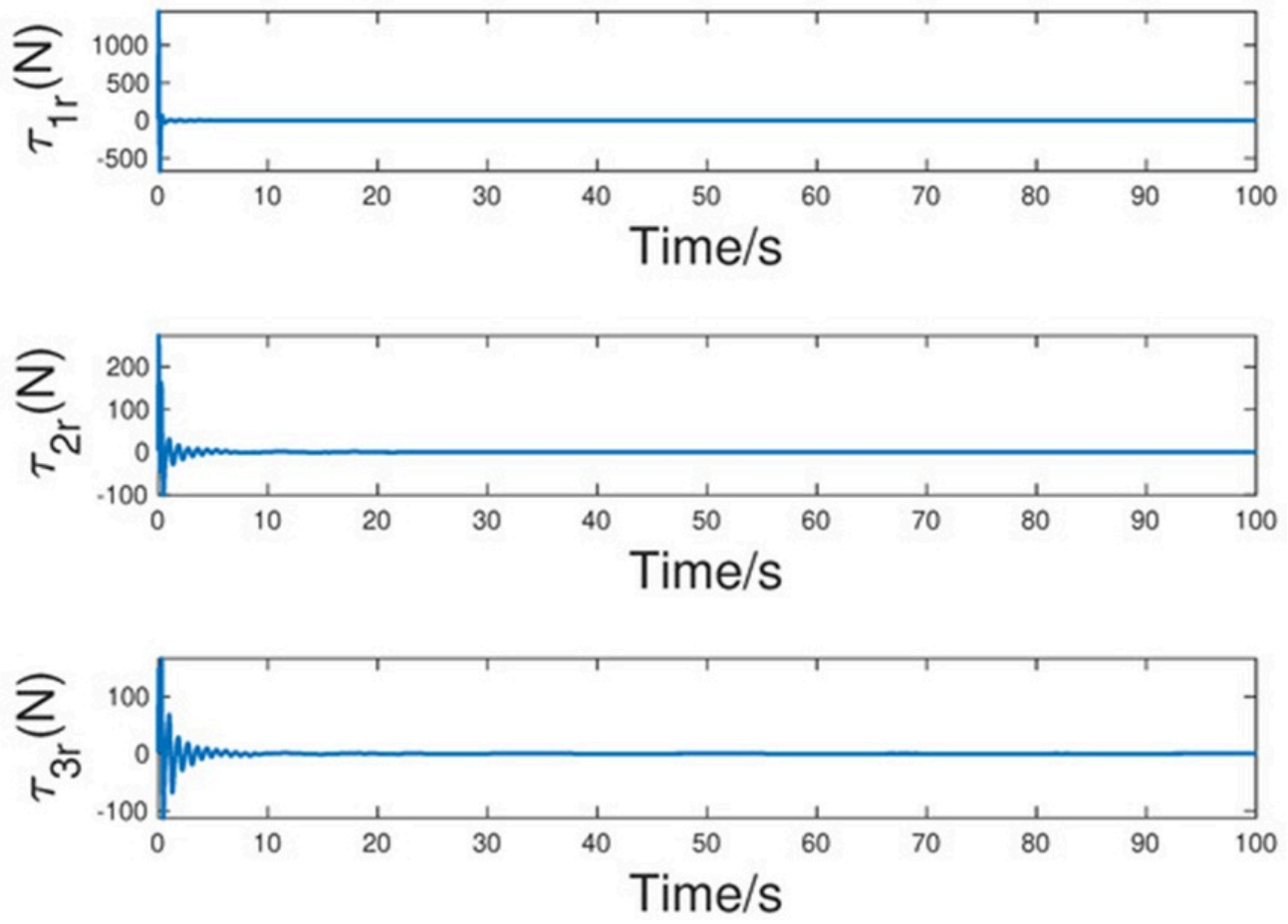

Figure 12. Output force (torque) variation curve of the actuator for the follower.

The simulation data indicate that the actual actuator output force settles into a stable state within 10 s. The approach proposed in this paper successfully nullifies the impact of actuator failure on the actual output force (torque) while maintaining the followers' formation-tracking fidelity.

A statistical breakdown of the event-triggered intervals for both the heading and speed controllers across the entire formation process is presented in **Table 2**. The shortest inter-trigger duration for the event-triggered controllers stands at 0.01 s (equaling one simulation timestep), while the longest inter-trigger duration reaches the order of seconds. The mean inter-trigger duration hovers around 0.11 s. Compared with traditional time-triggered controllers that operate at a fixed 0.01 s interval, the event-triggered mechanism drastically reduces the controller update rate.

Table 2. Event-triggering times of each UAV.

UAV No.	Velocity control time interval			Heading angle control time interval		
	Average time (s)	Maximum time (s)	Minimum time (s)	Average time (s)	Maximum time (s)	Minimum time (s)
UAV 1	0.118	2.390	0.010	0.124	0.970	0.010
UAV 2	0113	2.040	0.010	0.120	1.850	0.010
UAV 3	0.097	3.780	0.010	0.121	1.130	0.010

© 2023 The Author(s). | Published by Agro Intelligence Research Press

As illustrated in **Figures 13 and 14**, these figures depict the event-triggering instants for the heading angle and velocity controls, respectively. In the early stage of the simulation, notable mismatches exist between the three UAVs' speed and heading angles and their desired counterparts, prompting frequent controller invocations, as manifested by the tightly clustered points in the plots. To allow the UAVs to lock onto the desired speed and heading angles promptly, the controllers are updated rapidly. As elaborated earlier, after roughly 8 s, the UAVs' speed reliably matches the desired speed, following which the speed controller's triggering rate begins to taper off. Similarly, after about 14 s, the UAVs' heading angle synchronizes with the desired heading angle, and the heading controller's triggering rate thereafter steadily declines.

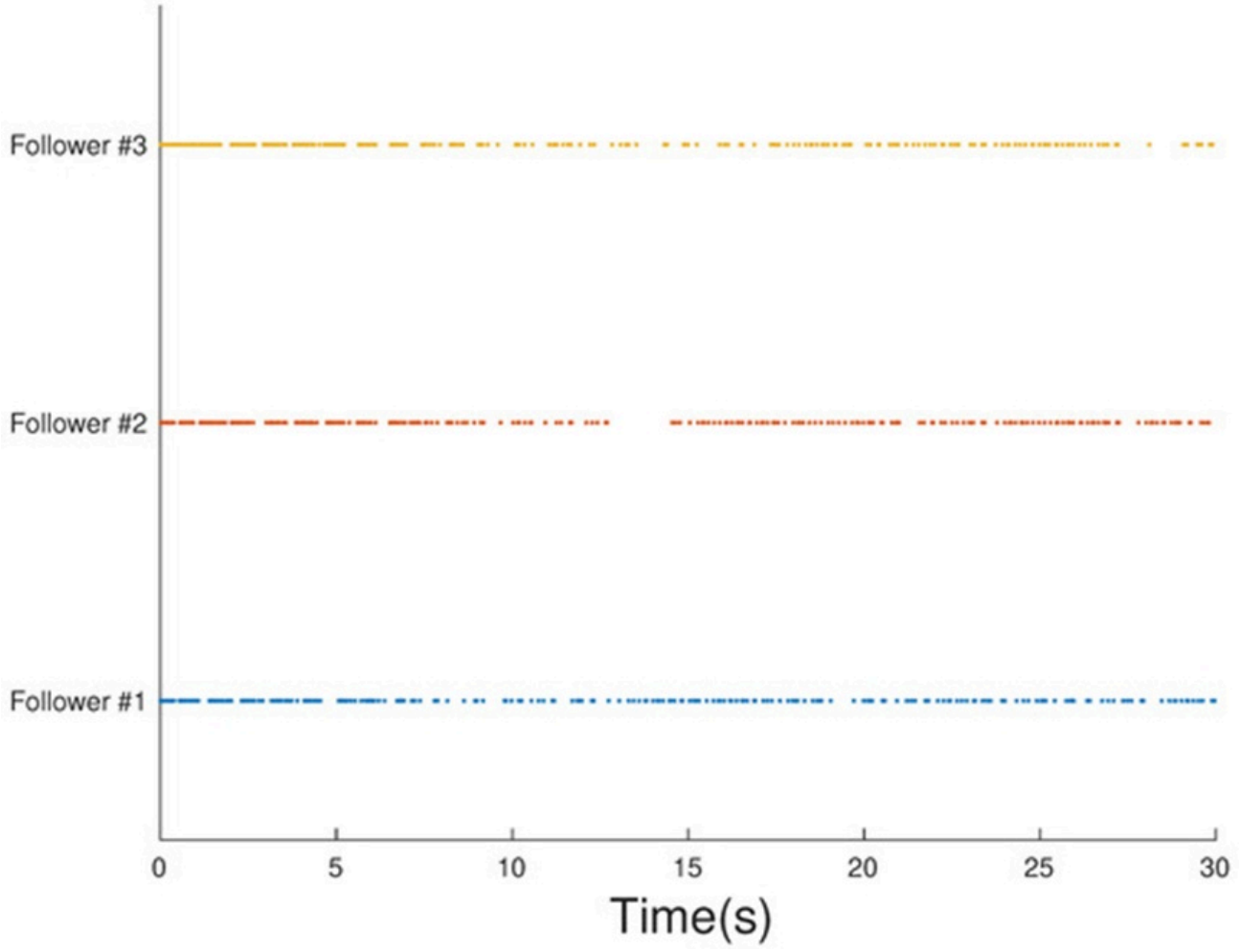

Figure 13. The event-triggering times for the heading angle control.

© 2023 The Author(s). | Published by Agro Intelligence Research Press

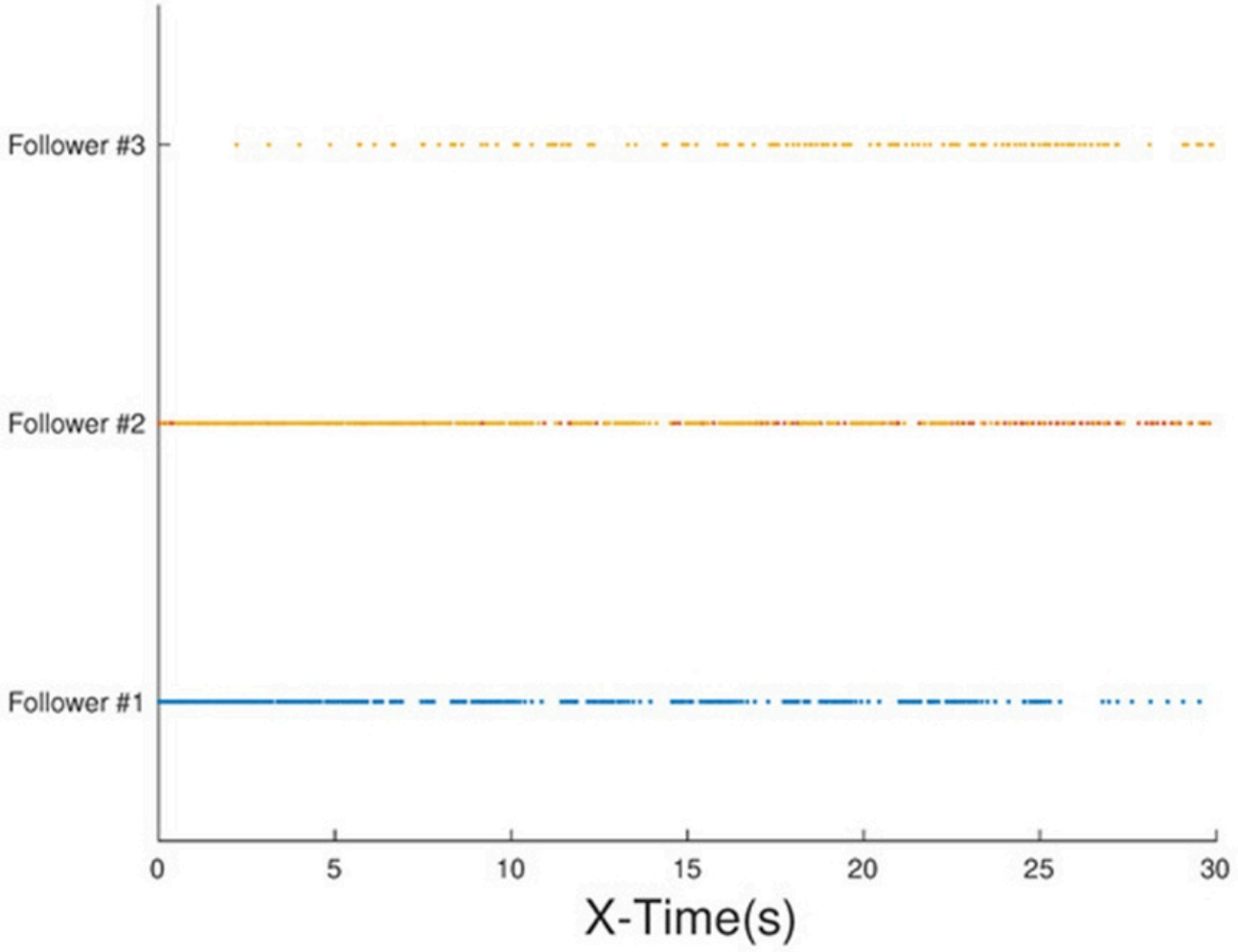

Figure 14. The event-triggering times for the velocity control.

As shown in **Figure 15**, this paper compares the triggering counts of the proposed event-triggered controllers with the total number of simulation steps. The yellow portion of the figure reflects the total simulation steps, equivalent to the triggering counts of time-triggered controllers. The red and blue portions, respectively, capture the triggering counts of the event-triggered heading angle controller and speed controller.

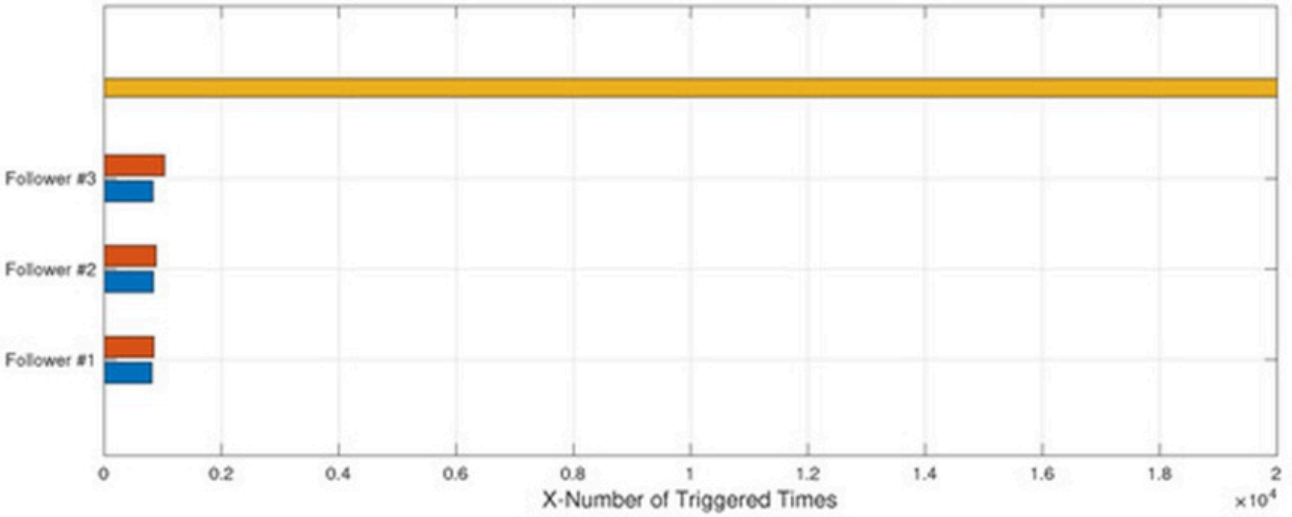

© 2023 The Author(s). | Published by Agro Intelligence Research Press

Figure 15. Contrast of triggered times.

As shown in **Figure 15**, the event-triggered controllers proposed in this work not only effectively fulfill the time-varying formation-tracking flight task but also substantially reduce the computational power and communication bandwidth requirements. In particular, the consumption of computational resources and communication bandwidth by UAVs 1, 2, and 3 amounts to just 8.2%, 8.6%, and 9.2%, respectively, of the time-triggered controllers' requirements. Consequently, under identical flight control computer hardware and communication resource limitations, the event-triggered controllers proposed herein can more efficiently meet the formation requirements of a considerably larger UAV swarm than time-triggered controllers. This yields a dramatic boost in the efficiency of flight control computer utilization.

Conclusion

This study proposes an event-triggered, fault-tolerant, time-varying formation control scheme that ensures predefined tracking performance for multiple UAVs. The methodology enforces predefined tracking performance, thereby strictly confining the convergence error within a designated bounded envelope. The formation-tracking guidance law is constructed, and a Lyapunov function is used to shape the tracking-error performance. Building on this, an adaptive tracking controller combining a neural network with an adaptive law is devised. The formation-tracking objective is fulfilled even under the simultaneous influence of actuator faults and external disturbances. An event-triggered control mechanism is also integrated to markedly improve the controller's solution efficiency. Lastly, simulation trials conducted across a range of operating conditions demonstrate that the proposed controller consistently drives the tracking error to converge within the prescribed range, regardless of external disturbances and internal actuator malfunctions.

Subsequent investigations may pursue experimental verification of the formation-tracking controller to gauge its practical efficacy. Such efforts would encompass subjecting the system to diverse environmental settings and assorted disturbance and fault configurations to substantiate its resilience and fault tolerance.

To address communication latency among UAVs and between UAVs and ground stations during real flight operations, future studies will leverage appropriate compensation strategies. For example, Liu *et al.* [49] present a robust, fault-tolerant tracking control framework based on a fixed-time disturbance observer. By combining Padé approximation with intermediate-variable techniques, this framework reduces the complexity of analyzing quadcopter UAV dynamics under input delays. The fixed-time disturbance observer design effectively neutralizes the impact of compounded disturbances, suggesting a promising research pathway for mitigating communication latency. Furthermore, to improve the convergence rate of the controller introduced in this paper, Liu and Wang [50] propose an innovative nonsingular fast terminal sliding-mode surface. The design intent behind this surface is to avert singularity issues while simultaneously strengthening controller performance and attaining swifter convergence. This methodology provides meaningful inspiration for accelerating the convergence speed of the controller developed herein, offering constructive insights for upgrading the overall system behavior.

Acknowledgements

None

Conflict of interest

None

Financial support

© 2023 The Author(s). | Published by Agro Intelligence Research Press

None

Ethics statement

None

Received: 03 Jun 2022 Revised: 08 Aug 2022 Accepted: 24 Aug 2022
Published online: 25 November 2023

Rights and permissions

Open Access The author(s) retain copyright. This article is licensed under the Creative Commons Attribution-NonCommercial-ShareAlike 4.0 International License. It may be shared and adapted for non-commercial purposes with appropriate attribution, an indication of changes, and distribution of adaptations under the same license. Third-party material may be subject to separate terms identified in its credit line. View the license at https://creativecommons.org/licenses/by-nc-sa/4.0/.

References

1. Muslimov TZ, Munasypov RA. Consensus-based cooperative control of parallel fixed-wing UAV formations via adaptive backstepping. Aerosp Sci Technol. 2021;109:106416.

2. Muslimov TZ, Munasypov RA. Adaptive decentralized flocking control of multi-UAV circular formations based on vector fields and backstepping. ISA Trans. 2020;107:143-59.

3. Wei L, Chen M, Li T. Disturbance-observer-based formation-containment control for UAVs via distributed adaptive event-triggered mechanisms. J Frankl Inst. 2021;358:5305-33.

4. Zhang Y, Li S, Wang S, Wang X, Duan H. Distributed bearing-based formation maneuver control of fixed-wing UAVs by finite-time orientation estimation. Aerosp Sci Technol. 2023;136:108241.

5. Chen J, Yang W, Shi Z, Zhong Y. Robust horizontal-plane formation control for small fixed-wing UAVs. Aerosp Sci Technol. 2022;131:107958.

6. Yan D, Zhang W, Chen H, Shi J. Robust control strategy for multi-UAVs system using MPC combined with Kalman-consensus filter and disturbance observer. ISA Trans. 2023;135:35-51.

7. Zhen Z, Zhu P, Xue Y, Ji Y. Distributed intelligent self-organized mission planning of multi-UAV for dynamic targets cooperative search-attack. Chin J Aeronaut. 2019;32:2706-16.

8. Hu J, Niu H, Carrasco J, Lennox B, Arvin F. Fault-tolerant cooperative navigation of networked UAV swarms for forest fire monitoring. Aerosp Sci Technol. 2022;123:107494.

9. Zhao Z, Niu Y, Shen L. Adaptive level of autonomy for human-UAVs collaborative surveillance using situated fuzzy cognitive maps. Chin J Aeronaut. 2020;33:2835-50.

10. Cai Z, Wang L, Zhao J, Wu K, Wang Y. Virtual target guidance-based distributed model predictive control for formation control of multiple UAVs. Chin J Aeronaut. 2020;33:1037-56.

11. Wang Y, Zhang T, Cai Z, Zhao J, Wu K. Multi-UAV coordination control by chaotic grey wolf optimization based distributed MPC with event-triggered strategy. Chin J Aeronaut. 2020;33:2877-97.

12. Guo S, Li Z, Niu Y, Wu L. Consensus disturbance rejection control of directed multi-agent networks with extended state observer. Chin J Aeronaut. 2020;33:1486-93.

13. Han L, Dong X, Li Q, Ren Z. Formation tracking control for time-delayed multi-agent systems with second-order dynamics. Chin J Aeronaut. 2017;30:348-57.

14. Liang Y, Dong Q, Zhao Y. Adaptive leader-follower formation control for swarms of unmanned aerial vehicles with motion constraints and unknown disturbances. Chin J Aeronaut. 2020;33:2972-88.

15. Yang W, Chen J, Zhang Z, Shi Z, Zhong Y. Robust cascaded horizontal-plane trajectory tracking for fixed-wing unmanned aerial vehicles. J Frankl Inst. 2022;359:1083-112.

16. Zhi Y, Liu L, Guan B, Wang B, Cheng Z, Fan H. Distributed robust adaptive formation control of fixed-wing UAVs with unknown uncertainties and disturbances. Aerosp Sci Technol. 2022;126:107600.

17. Lungu M. Auto-landing of UAVs with variable centre of mass using the backstepping and dynamic inversion control. Aerosp Sci Technol. 2020;103:105912.

18. Sun R, Zhou Z, Zhu X. Stability control of a fixed full-wing layout UAV under manipulation constraints. Aerosp Sci Technol. 2022;120:107263.

19. Zhang B, Sun X, Lv M. Distributed adaptive specified-time synchronization tracking of multiple 6-DOF fixed-wing UAVs with guaranteed performances. ISA Trans. 2022;129:260-72.

20. Chen K, Zhu S, Wei C, Xu T, Zhang X. Output constrained adaptive neural control for generic hypersonic vehicles suffering from non-affine aerodynamic characteristics and stochastic disturbances. Aerosp Sci Technol. 2021;111:106469.

21. Hu B, Guan ZH, Lewis FL, Chen CP. Adaptive Tracking Control of Cooperative Robot Manipulators With Markovian Switched Couplings. IEEE Trans Ind Electron. 2021;68:2427-36.

22. Yu Z, Zhang Y, Jiang B, Yu X, Fu J, Jin Y, et al. Distributed adaptive fault-tolerant close formation flight control of multiple trailing fixed-wing UAVs. ISA Trans. 2020;106:181-99.

23. Chen S, Chen Z. On Active Disturbance Rejection Control for a Class of Uncertain Systems With Measurement Uncertainty. IEEE Trans Ind Electron. 2021;68:1475-85.

24. Wang X, Guo J, Tang S, Qi S. Fixed-time disturbance observer based fixed-time back-stepping control for an air-breathing hypersonic vehicle. ISA Trans. 2019;88:233-45.

25. Dong C, Liu Y, Wang Q. Barrier Lyapunov function based adaptive finite-time control for hypersonic flight vehicles with state constraints. ISA Trans. 2020;96:163-76.

26. Su Z, Li C, Wang H. Barrier Lyapunov function-based robust flight control for the ultra-low altitude airdrop under airflow disturbances. Aerosp Sci Technol. 2019;84:375-86.

27. Liu K, Yang P, Wang R, Jiao L, Li T, Zhang J. Observer-based adaptive fuzzy finite-time attitude control for quadrotor UAVs. IEEE Trans Aerosp Electron Syst. 2023;59:8637-54.

28. Liu K, Yang P, Jiao L, Wang R, Yuan Z, Dong S. Antisaturation fixed-time attitude tracking control based low-computation learning for uncertain quadrotor UAVs with external disturbances. Aerosp Sci Technol. 2023;142:108668.

© 2023 The Author(s). | Published by Agro Intelligence Research Press

29. Huang Y, Wang J, Shi D, Shi L. Toward Event-Triggered Extended State Observer. IEEE Trans Autom Control. 2018;63:1842-9.

30. Zhen Z, Tao G, Xu Y, Song G. Multivariable adaptive control based consensus flight control system for UAVs formation. Aerosp Sci Technol. 2019;93:105336.

31. Yu Z, Zhang Y, Liu Z, Qu Y, Su C, Jiang B. Decentralized finite-time adaptive fault-tolerant synchronization tracking control for multiple UAVs with prescribed performance. J Frankl Inst. 2020;357:11830-62.

32. Xu B, Shi Z, Sun F, He W. Barrier Lyapunov Function Based Learning Control of Hypersonic Flight Vehicle with AOA Constraint and Actuator Faults. IEEE Trans Cybern. 2019;49:1047-57.

33. Yuan Y, Wang Z, Guo L, Liu H. Barrier lyapunov functions-based adaptive fault tolerant control for flexible hypersonic flight vehicles with full state constraints. IEEE Trans Syst Man Cybern Syst. 2020;50:3391-400.

34. Zhou W, Li J, Liu Z, Shen L. Improving multi-target cooperative tracking guidance for UAV swarms using multi-agent reinforcement learning. Chin J Aeronaut. 2022;35:100-12.

35. Abbaspour A, Yen KK, Forouzannezhad P, Sargolzaei A. A Neural adaptive approach for active fault-tolerant control design in UAV. IEEE Trans Syst Man Cybern Syst. 2020;50:3401-11.

36. Sun J, Yang J, Li S, Zheng WX. Sampled-Data-Based Event-Triggered active disturbance rejection control for disturbed systems in networked environment. IEEE Trans Cybern. 2019;49:556-66.

37. Hua Y, Dong X, Li Q, Ren Z. Distributed fault-tolerant time-varying formation control for high-order linear multi-agent systems with actuator failures. ISA Trans. 2017;71:40-50.

38. Yu Z, Zhang Y, Jiang B, Su C, Fu J, Jin Y, et al. Decentralized fractional-order backstepping fault-tolerant control of multi-UAVs against actuator faults and wind effects. Aerosp Sci Technol. 2020;104:105939.

39. Yu Z, Qu Y, Zhang Y. Distributed fault-tolerant cooperative control for multi-uavs under actuator fault and input saturation. IEEE Trans Control Syst Technol. 2019;27:2417-29.

40. Yu Z, Zhang Y, Jiang B, Yu X. Fault-Tolerant time-varying elliptical formation control of multiple fixed-wing uavs for cooperative forest fire monitoring. J Intell Robot Syst. 2021;101:1-15.

41. Yu Z, Qu Y, Zhang Y. Safe control of trailing UAV in close formation flight against actuator fault and wake vortex effect. Aerosp Sci Technol. 2018;77:189-205.

42. Administration FA. Pilot's handbook of aeronautical knowledge. skyhorse publishing inc. New York, NY, USA. 2009.

43. Bayezit I, Fidan B. Distributed cohesive motion control of flight vehicle formations. IEEE Trans Ind Electron. 2012;60:5763-72.

44. Karimoddini A, Lin H, Chen BM, Lee TH. Hybrid three-dimensional formation control for unmanned helicopters. Automatica. 2013;49:424-33.

45. Wang Y, Wang D, Zhu S. Cooperative moving path following for multiple fixed-wing unmanned aerial vehicles with speed constraints. Automatica. 2019;100:82-9.

46. Broomhead D, Lowe D. Radial Basis Functions, Multi-Variable Functional Interpolation and Adaptive Networks. Royal Signals and Radar Establishment Malvern. Worcestershire, UK. 1988.

47. Cruz-Zavala E, Moreno JA, Fridman LM. Uniform robust exact differentiator. IEEE Trans Autom Control. 2011;56:2727-33.

© 2023 The Author(s). | Published by Agro Intelligence Research Press

48. Su B, Wang H, Wang Y, Gao J. Event-triggered formation control for AUVs with fixed-time sliding mode disturbance observer. Control Decis. 2022;37:1116-26.

49. Liu K, Wang R, Zheng S, Dong S, Sun G. Fixed-time disturbance observer-based robust fault-tolerant tracking control for uncertain quadrotor UAV subject to input delay. Nonlinear Dyn. 2022;107:2363-90.

50. Liu K, Wang R. Antisaturation adaptive fixed-time sliding mode controller design to achieve faster convergence rate and its application. IEEE Trans Circuits Syst II Express Briefs. 2022;69:3555-9.

© 2023 The Author(s). | Published by Agro Intelligence Research Press